

Geology and Fluid Characteristics of the Mina Velha and Mandiocal Orebodies and Implications for the Genesis of the Orogenic Chega Tudo Gold Deposit, Gurupi Belt, Brazil *

EVANDRO L. KLEIN,[†]

Geological Survey of Brazil, Av. Dr. Freitas, 3645, Belém-PA, Brazil, CEP: 66095-110

JOSÉ W. A. RIBEIRO,

Newmont Overseas Exploration Limited, Surinam

CHRIS HARRIS,

Department of Geological Sciences, University of Cape Town, Rondebosch 7700, South Africa

CANDIDO A. V. MOURA,

Universidade Federal do Pará, Centro de Geociências, CP 1611, Belém-PA, Brazil, CEP: 66075-900

AND ANDRÉ GIRET

Université Jean Monnet, Département de Géologie, 23, rue du Docteur Paul Michelon, 42023, Saint Etienne, CEDEX 2, France

Abstract

The Chega Tudo gold deposit is located in the Gurupi belt of northern Brazil. Gold mineralization in the Mina Velha (upper level) and Mandiocal (intermediate and lower levels) orebodies is hosted in highly strained Paleoproterozoic (2148–2160 Ma) felsic to intermediate metavolcanic rocks and schists that record greenschist facies metamorphism. The orebodies are broadly concordant with the regional northwest-oriented foliation, and mineralization comprises thick quartz vein sets and small quartz-carbonate-sulfide veinlets and enclosing hydrothermally altered host rocks. The hydrothermal mineral assemblage is postpeak metamorphism, syn- to late tectonic, and includes quartz, calcite, chlorite, white mica, pyrite, subordinate chalcopryrite, and traces of sphalerite and galena.

Free-milling gold occurs in sulfide-poor veins in the upper and lower zones of the deposit, whereas refractory gold was deposited in fractures of pyrite and quartz in the more gold-enriched intermediate (\pm lower) level. Fluid inclusion and stable isotope (O, H, C, and S) data indicate that the two styles of gold deposition were produced by a combination of fluid immiscibility, fluid-rock reactions (sulfidation, carbonatization), and probably mixing, occurring in two discrete stages within a single mineralizing event associated with fluid flow within and around an active shear zone under fluctuating pressure conditions.

The refractory gold was deposited at 340° to 370°C from a CO₂-CH₄-H₂O-NaCl fluid having salinity of 5.8 \pm 2.7 wt percent NaCl equiv, variable CO₂ contents (typically 12–22 mol %), and up to 6 mol percent CH₄. The $\delta^{18}\text{O}$ and δD values of this fluid are 7.9 to 9.4 per mil and –29 to –37 per mil, respectively, indicating a metamorphic origin. Carbon isotopes show contrasting values in fluid inclusion CO₂ ($\delta^{13}\text{C} = -24.1\text{‰}$) and calcite ($\delta^{13}\text{C} = \text{of } -3.8\text{‰}$). The strongly negative value of fluid inclusion CO₂ is interpreted to be an organic signature acquired at the site of deposition by reaction of the deeply sourced ore-forming fluid with carbonaceous schists present in the deepest part of the deposit. The higher value for calcite probably records a crustal source. Oxygen fugacities calculated for the whole range of T-P-XCO₂ conditions yielded log f_{O_2} between –28.7 and –30.5, indicating reduced conditions for the fluid, which is in agreement with the mineral paragenesis, fluid inclusion compositions, and sulfur isotope values.

The second fluid, responsible for the deposition of the free-milling gold in veins and probably part of the gold of the lower zone of the deposit, had a lower temperature (330°–340°C). This CO₂-H₂O-NaCl fluid had a salinity of 1.6 to 2.5 wt percent NaCl equiv and contained 11 to 13 mol percent CO₂. The $\delta^{18}\text{O}$ and δD values of this fluid are 5.3 to 7.2 per mil and –12 to –30 per mil, respectively, also indicating a metamorphic source. The $\delta^{13}\text{C}$ value of fluid inclusion CO₂ is –6.9 per mil, likely representing a mantle-derived carbon source. Log f_{O_2} values between –30.5 and –31.5 also indicate slightly more reduced conditions for this fluid. Both fluids had near-neutral pH, between 5 and 6.2, and $\delta^{34}\text{S}$ values of H₂S between –0.2 and –1.0 per mil, interpreted to reflect derivation of sulfur from magmatic sulfides.

[†] Corresponding author: e-mail, eklein@be.cprm.gov.br

*A digital supplement to this paper is available at <http://www.geoscience.world.org/> or, for members and subscribers, on the SEG website, <http://www.segweb.org/>.

The Mina Velha and Mandiocchal orebodies represent different mineralization styles of the Chega Tudo deposit, and the determined conditions of ore formation may be related to two distinct events or to a single event with sequential stages of hydrothermal alteration and gold mineralization. The corresponding fluid properties, hydrothermal alteration, structural control, tectonic setting, geology, and metamorphism are analogous to those of orogenic gold deposits.

Introduction

THE GURUPI BELT in northern Brazil is a polyphase plutonic-metamorphic belt that contains a number of gold deposits and small undeveloped showings (Fig. 1). The exploitation of alluvial ores by small miners (*garimpo* mining) started in the 17th century, but reliable statistics on the historical production are not available. At least between 1965 and 1996, the cumulative *garimpo* production was about 16 tonnes (t) Au (Araujo Neto, 1998). This activity led to the recognition of primary ores, and after the 1980s several areas were developed by mining companies, including the Cachoeira, Chega Tudo, Cipoeiro, Montes Áureos, and Serrinha deposits (Figs. 1, 2) and a number of targets containing primary and paleoplacer gold. Chega Tudo and Cipoeiro are, so far, the most important deposits in the Gurupi belt, containing resources of about 60 t of gold grading 1.4 g/t Au (Torresini, 2000), whereas the Cachoeira deposit holds resources of ~20 t Au (Klein et al., 2005a).

The gold deposits of the Gurupi belt have many common characteristics (Torresini, 2000; Ribeiro, 2002; Yamaguti and Villas, 2003; Klein et al., 2005a, b, 2006a, 2007), which include (1) ore-hosting shear zones developed in an accretionary and/or continental margin setting, (2) host rocks that are dominantly greenschist facies volcanosedimentary rocks, and subordinate, altered tonalites having an age of 2148 to 2160 Ma, (3) a mineralization style characterized by abundant quartz-carbonate veins and surrounding pervasive hydrothermal alteration, with gold occurring both in veins and disseminated in the altered host rocks, (4) late timing with respect to granitic magmatism, metamorphism, and deformation, and (5) fluid inclusion and stable isotope compositions that are consistent between deposits. These characteristics are also very similar to those of typical greenstone-hosted orogenic lode gold deposits (e.g., Groves et al., 1998; McCuaig and Kerrich, 1998; Goldfarb et al., 2005).

Geologic and genetic aspects of the Cachoeira, Cipoeiro, Serrinha, and Montes Áureos deposits recently have been described by Torresini (2000), Ribeiro (2002), Yamaguti and Villas (2003), and Klein et al. (2005a, 2006a, 2007), and some geologic and structural aspects of the Chega Tudo deposit also have been discussed (Torresini, 2000; Ribeiro, 2002). However, no information is available concerning the genesis of the Chega Tudo deposit.

This paper provides data on the petrography, fluid inclusion, and stable isotope (O, H, C, and S) composition of alteration-related minerals from two parts of the Chega Tudo deposit, the upper Mina Velha, and intermediate and lower Mandiocchal orebodies (Figs. 2, 3). Based on the results and on available field and structural information, genetic aspects of this deposit are discussed, including fluid composition, P-T- f_{O_2} -pH conditions of the hydrothermal system, mechanisms for gold transport and deposition, and possible sources for the fluid and solutes.

Geologic Overview

Lithostratigraphy

Two major Precambrian geotectonic units, namely, the São Luís craton and the Gurupi belt, along with minor sedimentary basins, are recognized in the studied region, cropping out as tectonic and erosive windows within large Phanerozoic sedimentary basins (Fig. 1). The São Luís craton is composed of subduction-related calc-alkaline granitoids, represented by the Tromaí Intrusive Suite, that range in age from 2165 to 2149 Ma (Klein and Moura, 2001; Klein et al., 2005c) (except where stated, all ages reported here are single zircon Pb evaporation ages), and of younger muscovite-bearing, peraluminous granites, dated at 2086 ± 10 Ma (Palheta, 2001). Both the calc-alkaline and the peraluminous granitoids are massive to foliated and underwent low-grade metamorphism at a regional scale. Nevertheless, the primary igneous mineralogy and textures are largely preserved. The granitoids intruded the greenschist (\pm lower amphibolite) facies volcanosedimentary rocks of the 2240 Ma Aurizona Group (Klein and Moura, 2001). These rocks are mostly schists of variable compositions, showing a penetrative schistosity and local folding. The cratonic rocks have not been affected by any other thermal event after about 1900 Ma, according to Rb-Sr and K-Ar evidence (see Klein and Moura, 2001, for review). The São Luís craton has been interpreted as a Paleoproterozoic accretionary orogen, with the juvenile calc-alkaline granitoids and the supracrustal rocks formed in intraoceanic settings, whereas the peraluminous granites record the collisional phase of the orogen (Klein et al., 2005b), which is better represented in the nearby Gurupi belt. Age, composition, tectonic setting, and paleogeographic reconstructions all favor a correlation with the Eburnean granitoids and the Birimian volcanosedimentary sequences of the West African craton (Torquato and Cordani, 1981; Klein et al., 2005c; Klein and Moura, 2008).

The Gurupi belt borders the south-southwestern boundary of the São Luís craton (Fig. 1). It comprises north-northwest-south-southeast-trending volcanosedimentary and meta-sedimentary sequences that are tectonically intercalated with amphibolite facies gneisses and were intruded by different generations of granitoids. The volcanosedimentary sequence (Chega Tudo Formation) consists of alternating felsic to mafic volcanic rocks and detrital (\pm chert) sedimentary rocks that underwent metamorphism under greenschist to lower-amphibolite conditions (Yamaguti and Villas, 2003; Klein et al., 2005b). Most of the rocks show a well-developed schistosity and/or mylonitic fabric that dip at moderate to high angles, generally to the southwest. They are locally folded, especially within the Tentugal shear zone. Felsic metavolcanic rocks have zircon ages of 2148 to 2160 Ma (Klein and Moura, 2001) interpreted as the crystallization ages of the volcanic protoliths, whereas Sm-Nd model ages (T_{DM}) are in the 2.20 to 2.28 Ga range, with positive ϵ_{Nd} values (Klein et al., 2005b). This indicates a juvenile character for these volcanic rocks,

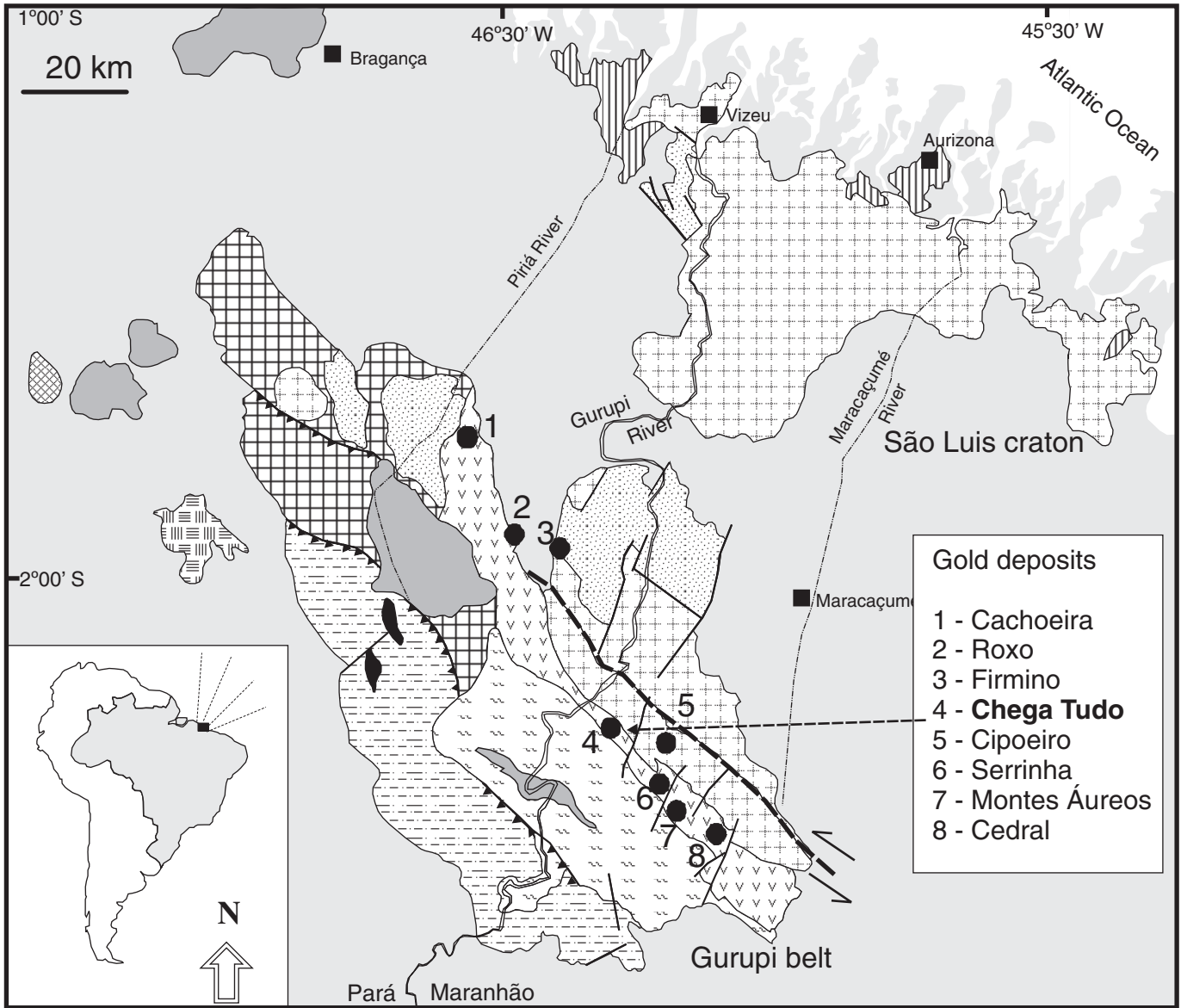


FIG. 1. Simplified geologic map of the São Luís craton and Gurupi belt showing the location of the Chega Tudo and other gold deposits (adapted from Klein et al., 2005b).

interpreted as having formed in arc-related systems associated with the Paleoproterozoic calc-alkaline and supracrustal rocks of the São Luís craton. Two metasedimentary sequences are considered here. The Gurupi Group is composed of detrital rocks of variable composition, including carbonaceous phyllite and schist, and coarser-grained quartz-mica

schist, recording metamorphism under sub- to upper-green-schist conditions (Costa, 2000). The stratigraphic age of this sequence is still uncertain. It is tentatively considered older than 2159 Ma, based on inferred intrusive relationships (Costa, 2000; Palheta, 2001) with granitoids of this age. The second sedimentary succession comprises amphibolite facies

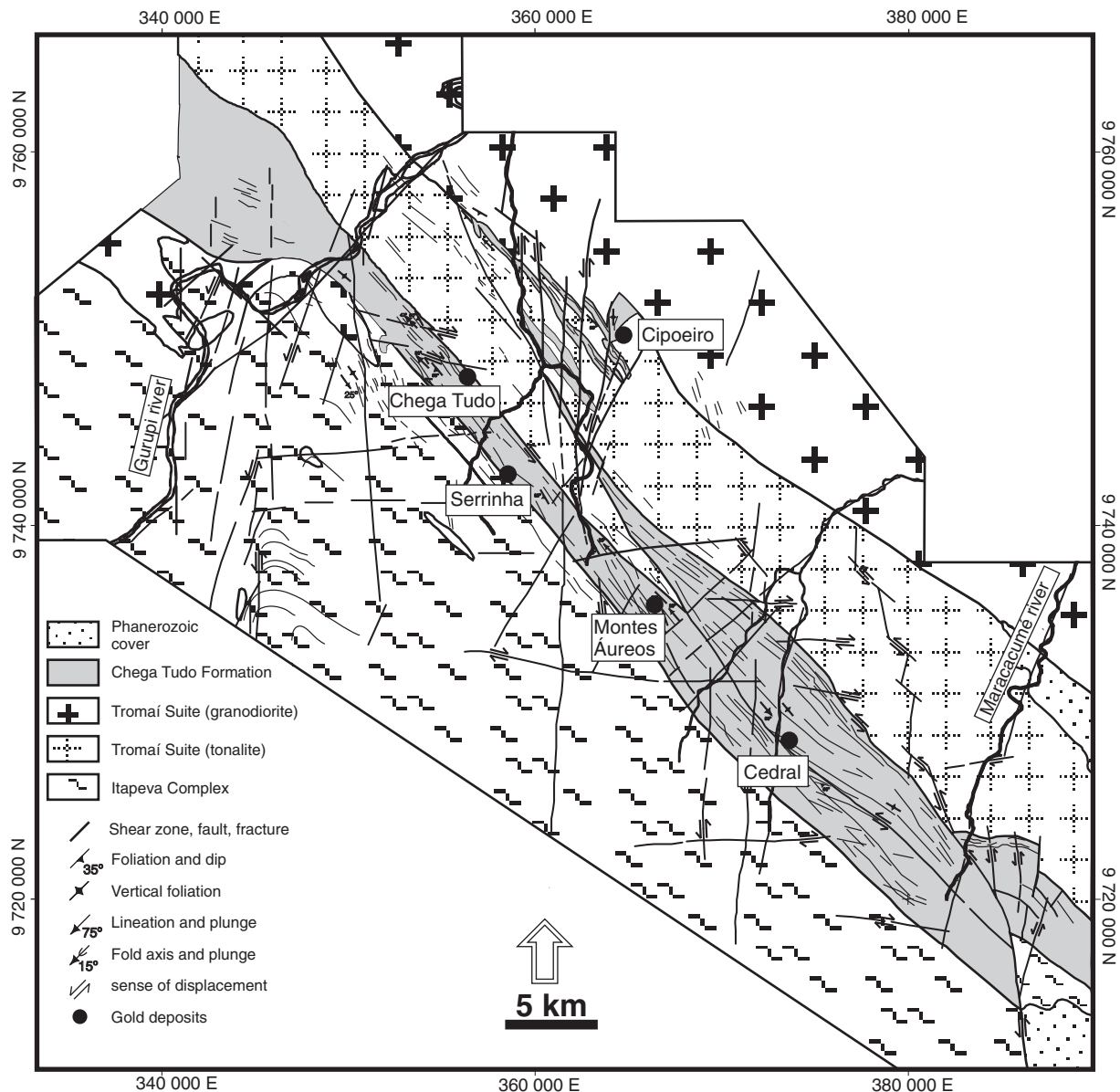


FIG. 2. Geologic map of the southeastern Gurupi belt (adapted from Ribeiro, 2002).

schists and feldspathic to aluminous quartzites grouped in the Marajupema Formation. The youngest detrital zircon of this unit, with an age of 1100 Ma, defines the maximum depositional age for the sediments (Klein et al., 2005b).

Orthogneisses of the Itapeva Complex are tectonically intercalated with the supracrustal rocks (Fig. 1). The gneisses are middle to upper amphibolite facies, foliated and banded rocks that show localized migmatization. A tonalite gneiss has a zircon age of 2167 ± 2 Ma (U-Pb ID-TIMS), interpreted as the age of crystallization of the igneous protolith of the gneiss (Klein et al., 2005b). Small lenses of granoblastic metatonalite to gneiss have an Archean age of 2594 ± 3 Ma (Klein et al., 2005b).

Granitoids of variable chemical affinities and ages intruded and/or were tectonically intercalated within the supracrustal sequences and the gneisses. Large wedges of the calc-alkaline

granitoids have been strongly affected by the Tentugal shear zone in the boundary zone between the São Luís craton and the Gurupi belt and have been incorporated into the framework of the belt (Pastana, 1995; Ribeiro, 2002), showing intense mylonitic foliation. Peraluminous, muscovite-, and biotite-bearing granites are relatively widespread (Fig. 1). They show variable effects of deformation, from a weak schistosity to a penetrative mylonitic fabric, depending on their position relative to deformation zones. Zircon ages of these granites are 2100 to 2080 Ma, with inherited ages in the range of 2325 to 2459 Ma and T_{DM} model ages between 2.09 and 3.23 Ga, with weakly negative to positive ϵ_{Nd} values indicating that both Paleoproterozoic and Archean crustal protoliths were involved in the origin of the granites (Palheta, 2001; Klein et al., 2005b). At least one of these granites shows field relationships that indicate syntectonic emplacement (Klein et al., 2005b).

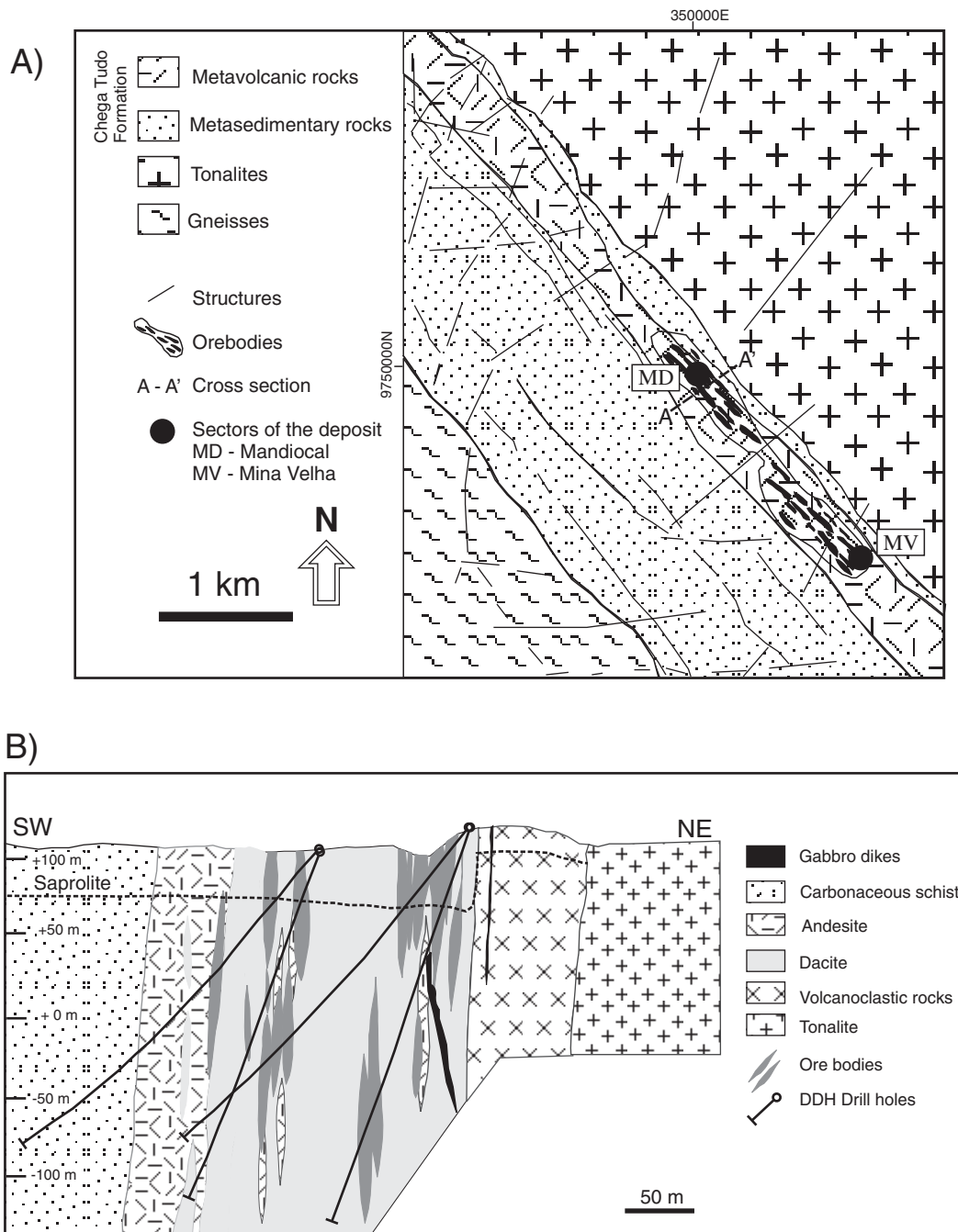


FIG. 3. A. Geologic map of the Chega Tudo deposit (after Torresini, 2000). B. Cross section of the Mandiocal orebody (modified from Torresini, 2000, and Ribeiro, 2002).

The Ney Peixoto granite (Fig. 1) is similar to the peraluminous granitoids described above. However, zircon dating indicates that this granite was emplaced in the Neoproterozoic at 549 ± 4 Ma (Palheta, 2001). An isolated body of metamorphosed nepheline-syenite is also of Neoproterozoic age and crops out within the Phanerozoic sedimentary cover. This body shows gneissic banding without any observed contact relationships (Fig. 1). A concordant zircon age of 732 ± 7 Ma (U-Pb, LAM-ICP-MS) was obtained by Klein et al. (2005b) and interpreted as the emplacement age of the nepheline

syenite. In addition to these two Neoproterozoic intrusions, most of the Paleoproterozoic units of the Gurupi belt show some imprint of a Neoproterozoic event, recorded by mineral Rb-Sr and K-Ar data, mostly in the range of 520 to 670 Ma (Almeida et al., 1968; Villas, 1982), in clear contrast to the cratonic area. Small sedimentary basins formed in depressions of both the São Luís craton and the Gurupi belt (Fig. 1) and likely represent postorogenic (molassic?) basins related to the final stages of Neoproterozoic events (Klein et al. 2005b, c).

Integrated geologic and geochronologic data suggest that the rocks of Gurupi belt and of the nearby São Luís craton had a common orogenic evolution in the Paleoproterozoic (Rhyacian). Juvenile, arc- and subduction-related processes occurred early in this period during the accretionary phase of the orogenesis between 2167 and 2150 Ma and are recorded in the widespread calc-alkaline magmatism represented by the batholiths of the Tromaí Intrusive Suite and metavolcanic rocks present in the Aurizona Group and Chega Tudo Formation. The Gurupi belt records the collisional phase of the orogenesis, probably along a continental margin, which was the locus of emplacement of peraluminous granitoids and of extensive metamorphism and deformation between 2100 and 2080 Ma. This evolution and the age intervals are largely coincident with the Transamazonian and Eburnean orogenies that are widespread in the South American platform and West African craton, respectively. This crustal block amalgamated in the Paleoproterozoic and was rifted in the Neoproterozoic, as indicated by the intrusion of the nepheline syenite at 732 Ma. The newly formed rift probably evolved into a continental margin that subsequently closed during the Brasiliano–Pan-African orogenies (Klein et al., 2005b, c).

Structural framework

Most of the gold deposits and showings of the Gurupi belt, including Chega Tudo, are hosted in structures associated with the strike-slip, sinistral Tentugal shear zone (Figs. 1, 2). This major structure consists of a ~15-km-long and 15- to 30-km-wide corridor of shear zones with variable structural aspects developed under ductile-brittle and greenschist facies conditions. Integrating structural and lithologic mapping with geophysical and radar imagery information, Ribeiro (2002) recognized a corridor of highly strained rocks striking dominantly N 40° W and characterized by concentrated strain and displacements reflecting distinct rheology or competency contrasts. The highly strained rocks correspond to metapelites and metavolcanic rocks of the Chega Tudo Formation (Klein et al., 2005b), whereas the less deformed rocks correspond to coarse-grained tonalites (Tromaí Intrusive Suite) and quartz-feldspathic schists (Gurupi Group²) to the northeast and southwest, respectively. Ribeiro (2002) also described a complex and protracted structural evolution for the region, with the N 40° W-trending structures transposed by north-northwest–south-southeast-trending ductile structures, along with the formation of a north-south–striking fault system and associated splays that have subsequently been reactivated and displaced by small-scale thrusts and east-west-oriented strike-slip faults.

A problem that stems from this complexity and from the polycyclic evolution of the Gurupi belt is the difficulty in determining unequivocally whether the structural features have been produced during a single and progressive deformational event or whether they represent two or more events. From field relationships and geochronologic information it is clear that a metamorphic event and associated intrusion of at least one syntectonic body of peraluminous granite occurred at about 2080 to 2100 Ma (Klein et al., 2005b). However, in Neoproterozoic time, all these Paleoproterozoic rocks had their Rb-Sr and K-Ar systems reset to some extent by the Brasiliano–Pan-African orogenies.

Metamorphism

The rocks of the Chega Tudo Formation, which hosts the Chega Tudo deposit and most of the gold mineralization of the Gurupi belt, have been variably metamorphosed from subgreenschist to lower amphibolite, but predominantly greenschist facies conditions. The metamorphic assemblages consist mostly of chlorite-sericite, chlorite-carbonate-epidote, chlorite-biotite-epidote-actinolite-muscovite-albite, and chlorite-biotite-plagioclase-amphibole, from the lowest to the highest grades (Pastana, 1995; Ribeiro, 2002; Yamaguti and Villas, 2003). The peak metamorphic conditions attained temperatures and pressures of 420° to 450°C and 2 to 3 kbars, respectively (Yamaguti and Villas, 2003). This metamorphic event is estimated to have occurred at about 2080 to 2100 Ma, based on the age of emplacement of the muscovite-bearing (collision-related) peraluminous granitoids (Palheta, 2001; Klein et al., 2005b).

Deposit Geology and Gold Mineralization

The Chega Tudo deposit comprises a series of discontinuous orebodies that are confined to highly strained rocks related to 50- to 150-m-wide shear zones developed over the volcanosedimentary rocks of the Chega Tudo Formation at the zone of contact between this formation and tonalites of the Tromaí Intrusive Suite (Fig. 2). This set of orebodies extends to over 2,000 m in length and to at least 200 m in depth (Fig. 3). The orebodies are broadly conformable to the subvertical mylonitic foliation, parallel to the strike and having irregular to lens and cigar shapes (Torresini, 2000; Ribeiro, 2002).

Gold mineralization occurred in two parallel domains, in metavolcanic and metasedimentary rocks, that show some differences in the structural and mineralogical characteristics. In the metasedimentary domain the mineralization is hosted in schists composed of quartz, sericite, and millimeter-thick layers of magnetite, and in subordinate carbonate and sericite-chlorite-bearing schists (Ribeiro, 2002). The mineralized zone is rather restricted and discontinuous and consists of small, fracture-filling veinlets of quartz, calcite, and pyrite that are concordant with the foliation. This style is similar to that described for the Serrinha deposit (Klein et al., 2006a) located southeast of Chega Tudo. Hydrothermal magnetite is also present and more abundant than pyrite, possibly derived from remobilization of sedimentary magnetite of the host rocks. Late-stage gabbro dikes are also hydrothermally altered, with the development of epidote, sericite, and especially chlorite. This rock is only weakly mineralized and regarded as waste (Torresini, 2000; Ribeiro, 2002).

This study is concentrated on the Mina Velha and Mandioc orebodies of the Chega Tudo deposit (Figs. 2, 3), which are representative of the more important styles of mineralization of the metavolcanic domain.

Mina Velha orebody

The Mina Velha orebody is characterized by vein-style mineralization and only the surface portion of the vein has been sampled. Gold is contained in a set of massive milky quartz veins (Fig. 4A), each approximately 50 cm in thickness and 20 to 100 m in length. These veins have subvertical dips and

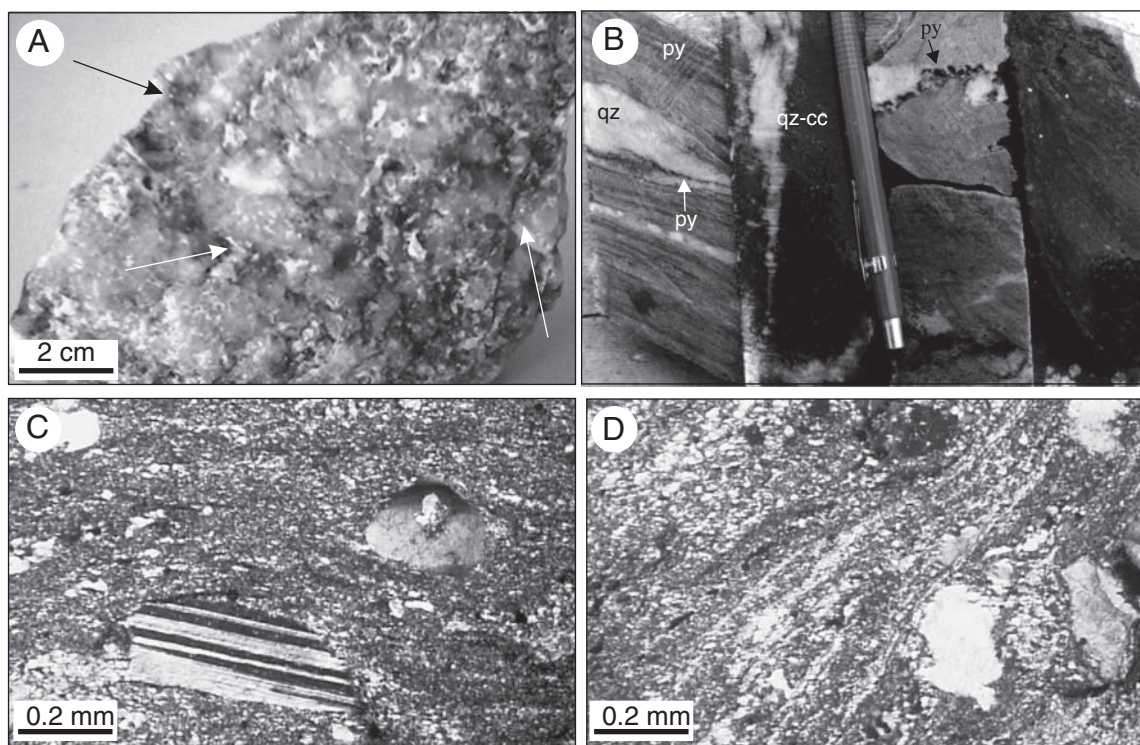


FIG. 4. Images of vein and host rocks of the Chega Tudo deposit. A. Massive milky quartz vein with visible gold particles and aggregates (arrows). B. Drill core slabs showing aspects of the mineralization and host rocks. Quartz and quartz-calcite veinlets hosted in deformed rhyodacite and dacite. Pyrite is distributed along fractures, foliation, and as disseminations. C. Photomicrograph of deformed dacite showing large porphyroclasts of quartz and plagioclase set in a sulfidized mylonite matrix. D. Photomicrograph of deformed dacite with quartz porphyroclasts set in sericite-rich mylonite matrix. Mineral abbreviations: cc = calcite, py = pyrite, qz = quartz.

strike to N 35° W. Collectively, they form a set of en echelon veins that are broadly conformable with the regional foliation and the local mylonitic fabric (N 40°–45° W/80°–85° SW), corresponding to oblique shear veins, in the sense of Hodgson (1989), that have been reoriented parallel to the shear zone walls during progressive deformation.

The host rock is a magnetite-bearing quartz-sericite schist with interlayered tuffs and felsic to intermediate metavolcanic rocks. Narrow halos composed of seams of white mica surround the veins. Free gold is commonly visible (Fig. 4A), especially at the vein-wall rock contacts as aggregates or irregularly shaped particles of <1 mm, but this gold lacks any clear association with concentrations of sulfide minerals.

Mandiocal orebody

In the Mandiocal orebody, diamond drilling attained a depth of ~140 m, intersecting several mineralized zones. Two representative zones have been sampled for this study at level 69–77m, grading >1 ppm (here referred to as the intermediate zone), and at level 96–97m, grading ~0.5 ppm near the contact with the metasedimentary domain (here referred to as the lower zone). In both the intermediate and lower zones, the mineralization consists of millimeter- to centimeter-thick quartz (±calcite, ±sulfide) veinlets and enclosing altered host rocks. The gold-bearing veinlets are located mostly within the foliation of the highly strained host dacite, but they also cut across the foliation (Fig. 4B).

The host rock to the mineralization is predominantly dacite porphyry, along with minor rhyolite, andesite, and volcanoclastic rocks (Figs. 3B, 4B). The dacite contains porphyroclastic quartz and more or less saussuritized plagioclase set in a fine-grained mylonitic matrix (Fig. 4C, D) composed of quartz, plagioclase, K-feldspar, and minor biotite. Preserved primary volcanic textures are found in less deformed lenses between highly strained zones. The metamorphism of the volcanic rocks produced an assemblage composed essentially of quartz, sericite, chlorite, carbonate, and epidote.

The pervasive hydrothermal alteration associated with the gold mineralization overprinted the metamorphic assemblage. This is indicated by veining, syntectonic crystallization of minerals in foliation planes, replacement and texturally destructive alteration, an increase in modal proportions of alteration minerals, and development of bleached zones that obscure the metamorphic texture. In addition to gold, the hydrothermal assemblage is composed of variable proportions of quartz, chlorite, white mica, calcite, and sulfide minerals, and the interpreted paragenesis is shown in Figure 5.

A complex brittle-ductile deformation history is indicated by changes in the thickness of the veinlets, undulose extinction of quartz of variable intensities, grain-size reduction, recrystallization, development of mosaics of hexagonal grains, and fracturing. In places, quartz occurs as large crystals, more or less preserved from plastic deformation. Fibrous aggregates of quartz, locally accompanied by chlorite, also are commonly

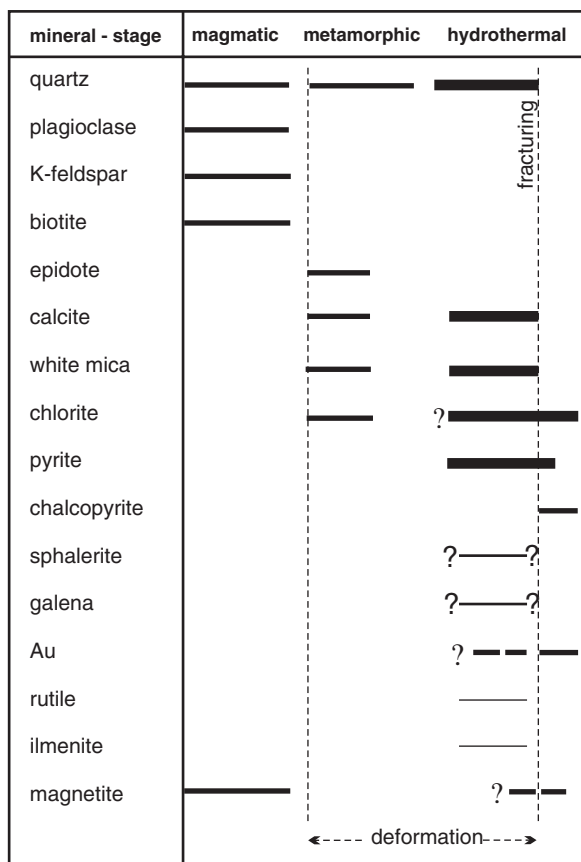


Fig. 5. Paragenetic sequences in distinct stages of the host rocks of the Chega Tudo deposit. The thickness of the lines indicates the importance of the mineral in the hydrothermal paragenesis.

found in pressure shadows of large pyrite crystals (Fig. 6A, B). The development of these pressure shadows is ascribed to diffusional solute transport in a deforming rock at low metamorphic grade, implying high fluid pressures with dissolution at the high pressure side of pyrite and precipitation at the low pressure side (Passchier and Trow, 1996). These features also indicate crystallization during the latest stages of deformation and foliation development (Witt, 1993). Moreover, the thickness of the quartz veinlets varies along strike, also suggesting a relationship between vein emplacement and the development of the hosting structure (Robert and Poulsen, 2001).

Chlorite occurs in a variety of textures and associations; most of the crystals have the longest dimension parallel to the foliation planes, whereas other grains crystallized in fractures of pyrite crystals and, in places, in association with quartz in pressure shadows of large pyrite crystals (Fig. 6A-D). White mica occurs mostly as aggregates of fine- to medium-grained crystals that define the foliation both in the host rock and in the veinlets (Fig. 6C). Calcite is only a minor constituent of the veinlets (<5 vol %), occurring in association with chlorite, white mica, and sulfides.

Pyrite is by far the predominant sulfide mineral, occurring in all the studied samples. Two generations of pyrite have been recognized, and both contain traces of Au (\pm Bi, As, Sb, and Te) as detected by scanning electron microscope with

semiquantitative energy dispersive system analysis (SEM-EDS). Early pyrite (Fig. 6A, B) is made up of large subhedral to euhedral crystals disseminated in the host rocks. As noted above, some crystals have fractures filled with chlorite (Fig. 6D) and commonly quartz and chlorite in pressure fringes. A later stage of pyrite is, in general, fine grained and has very small inclusions of ilmenite and rutile. It forms aggregates and stringers within the foliation planes and within fractures of the quartz veinlets, and disseminations in the host rocks, where it is associated with quartz, calcite, and white mica (Fig. 6C, E). It is possible that the later stage of pyrite formed at the expense of the early-stage pyrite through dissolution and reprecipitation during deformation.

Sphalerite and galena have been recognized by SEM imagery only as very fine inclusions (<60 μ m) in pyrite or as individual minerals in equilibrium with pyrite (Fig. 6F) in samples of the intermediate zone. Chalcopyrite is also a very subordinate phase and is more abundant in the lower zone. However, minor amounts of chalcopyrite precipitated in fractures in pyrite together with gold (Fig. 6G). Magnetite has been observed in a few samples where it is spatially associated with sulfides, but only rarely in physical contact with the sulfides, and it is much more abundant in the lower zone.

Gold occurs in association with sulfide concentrations as microscopic, irregularly shaped, and undeformed particles that precipitated in fractures in pyrite and quartz (Fig. 6G, H). Traces of gold also have been detected by SEM-EDS analysis of pyrite and galena, and rarely in sphalerite of the intermediate zone.

Locally, the hydrothermal alteration shows an asymmetric zoning at the centimeter scale (Fig. 6E). In this case, quartz veinlets are surrounded by proximal calcite (\pm pyrite), an intermediate chlorite-rich zone composed of chlorite, quartz, calcite, white mica, and pyrite, and a distal zone composed of white mica, quartz, pyrite, and minor calcite. As a whole, calcite contents increase and white mica contents decrease toward the vein.

Timing of Gold Mineralization

The petrographic and structural evidence suggest that the hydrothermal alteration was syn- to late tectonic with respect to development of the hosting structures and occurred after the peak of metamorphism. The relative timing of gold mineralization is constrained by the presence of undeformed gold particles in the vein-wall rock contacts at Mina Velha, and in fractures of quartz and pyrite crystals in the intermediate and lower zones at Mandiocal. These features indicate that mineralization was associated with a brittle episode that occurred late in the structural evolution of the host rocks. The relative timing of vein- and sulfide-hosted gold is, however, uncertain.

The absolute timing of gold mineralization also is unknown. The minimum age of the host metavolcanic rocks is 2148 ± 1 Ma (Klein and Moura, 2001). Preliminary step-leaching Pb-Pb dating of ore-related sulfides of the Cachoeira deposit (Klein et al., 2006b), which is hosted in the same formation as Chega Tudo, does not record a Neoproterozoic event, and model and isochron ages are \sim 2000 Ma. Since the mineralization is post-metamorphic, the age of the Paleoproterozoic metamorphism in the Gurupi belt (2080–2100 Ma) is a maximum age for the

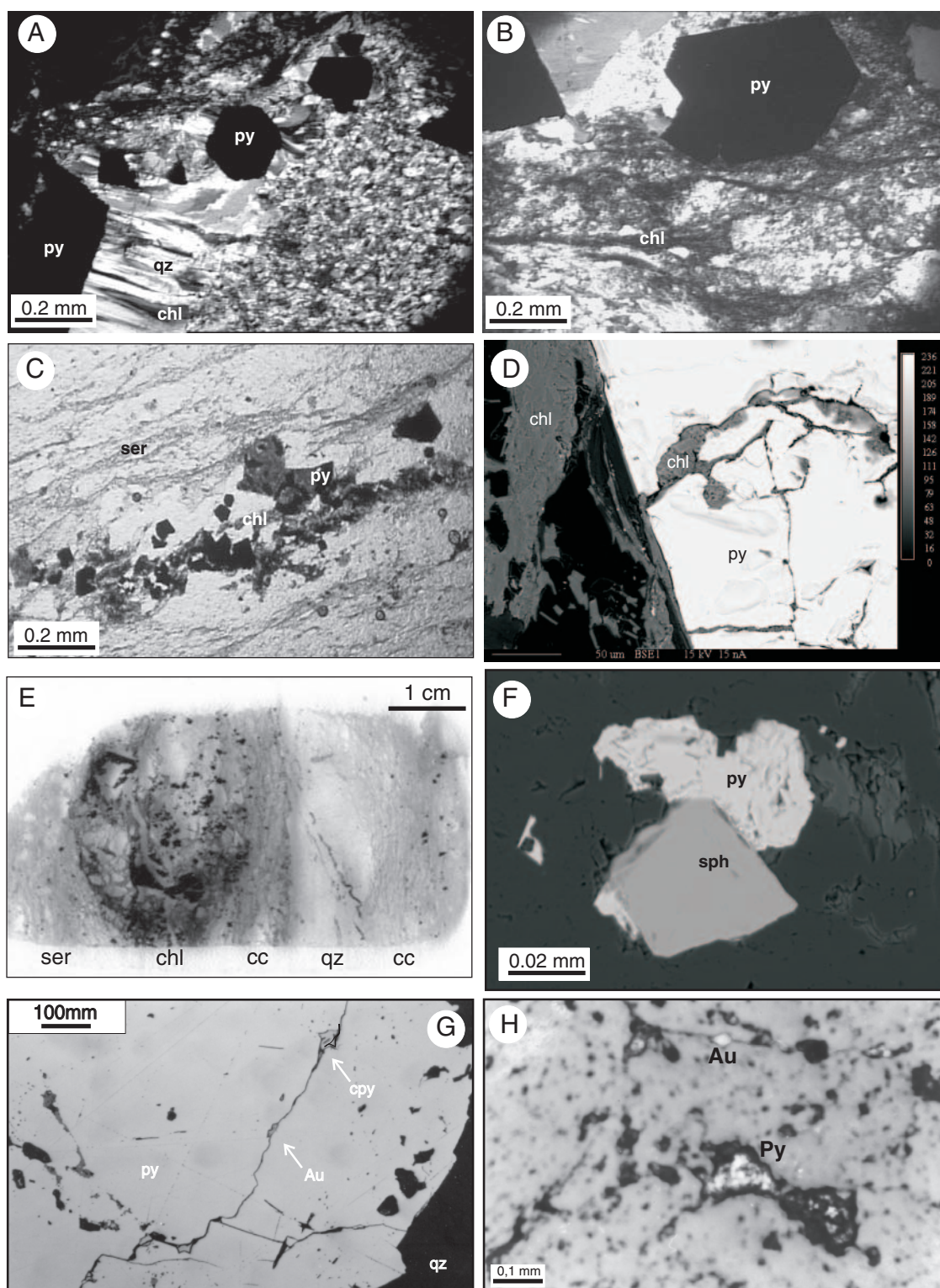


FIG. 6. Textural features of the host rocks and hydrothermal alteration of the Mandiocal orebody of the Chega Tudo deposit. A. Large pyrite crystals (black) with pressure fringe composed of quartz and chlorite, set in a fine-grained hydrothermal matrix. B. Seams of chlorite defining the foliation in an altered dacite. C. Deformed quartz veinlet (white) from level 77m, with auriferous pyrite stringers and seams of sericite defining the foliation. D. Backscattered electron (BSE) image showing chlorite crystals at the margins and in fractures of a large pyrite grain. E. Polished slab from level 96.5m showing the zoned alteration, with a quartz veinlet surrounded by a proximal calcite-rich zone, intermediate chlorite-rich zone, and distal sericitic zone. F. BSE image showing coexisting pyrite and sphalerite. G. Photomicrograph of a pyrite crystal with a fracture filled with gold and chalcopyrite. H. Gold and pyrite crystals in fractures of quartz. Mineral abbreviations: Au = gold, cc = calcite, chl = chlorite, cpy = chalcopyrite, py = pyrite, qz = quartz, ser = sericite (white mica), sph = sphalerite.

mineralizing episode. Assuming the probable correlation between the Gurupi region and the Eburnean-Birimian sequences of the West-African craton (Klein and Moura, 2008), this time interval is in reasonable agreement with the ages of 2014 to 2098 Ma (Marcoux and Milési, 1993; Oberthür et al., 1998) estimated for other gold deposits in that craton.

Sampling and Analytical Methods

Microprobe analysis of chlorite was carried out at the Université Blaise Pascal in Clermont Ferrand, France, using a Cameca SX-100 probe, coupled with a backscattered electron (BSE) system. Acceleration voltage was 15 kV, with 10 seconds counting time per element. Calibration was done with available natural and synthetic standards. FeO was considered as total iron and H₂O was calculated by stoichiometry. The analytical results were recalculated on the basis of 36 oxygen atoms (O, OH), 16 OH groups, and 8 atoms of Si + Al^{IV} (i.e., based on 28 atoms of oxygen equivalent).

Fluid inclusion studies were carried out on quartz from thick veins and small quartz ± carbonate veinlets. Sample preparation and analytical procedures followed recommendations of Roedder (1984) and Shepherd et al. (1985). After petrographic examination, the microthermometric work was performed using a Chaixmeca heating-freezing stage at the Universidade Federal do Pará (UFPA), in Belém, Brazil. Calibration was done with synthetic CO₂ and H₂O standards. Precision was estimated to be ±0.3°C for runs below 40°C and ±3°C for runs above 40°C. Raman analyses were carried out at the Universidade Federal de Minas Gerais (UFMG), in Belo Horizonte, Brazil, using a Dilor XY spectrometer equipped with multiple collectors. The excitation source was an Argon laser Ivanova 70-3 with a wavelength of 514.53 nm and 150 mW of power. Integration time was 10 seconds, with 10 accumulations for each spectral line. Calibration was done with mercury light and tests were performed for CO₂, CH₄, H₂S, and N₂.

Carbon, oxygen, and hydrogen isotope analyses were carried out at the Laboratoire des Isotopes Stables of the Université Jean Monnet (UJM) in Saint Etienne, France. Isotope ratios were measured using a Micromass-Isoprime gas-source mass spectrometer in dual-inlet mode. For carbonates, about 5 to 10 mg of dry powders were used for isotopic determinations. The samples were reacted overnight in vacuum at 25.2°C (McRae, 1950) with 2 ml of H₃PO₄ (100%). Analysis of duplicates produced differences of more than 0.2 per mil for both δ¹³C and δ¹⁸O, and the calcite-phosphoric acid fractionation factor of 1.01025 (Friedman and O'Neil, 1977) was used in the correction procedure. Silicate minerals for oxygen and hydrogen analysis and sulfide minerals for sulfur analysis were separated by conventional magnetic and heavy liquids techniques and handpicked under binocular microscope. When carbonate minerals were present, they were removed by reaction with HCl. All mineral separates were estimated to be >95 percent pure. For oxygen isotope analysis of silicate minerals, two methods were employed, both using BrF₅ as reagent. The conventional fluorination method (Clayton and Mayeda, 1963) was employed for hydrated minerals, and a CO₂ laser fluorination system (Harris et al., 2000) was used for quartz analysis. In both methods oxygen was converted to CO₂ by reaction with graphite. In the conventional method,

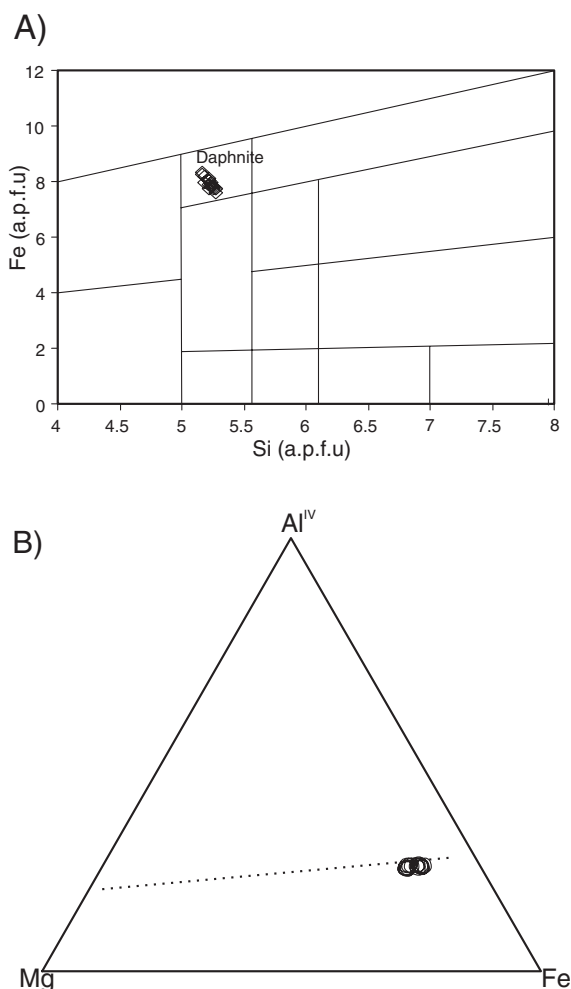
samples were loaded into Ni reaction vessels and degassed at 250°C for about 2 hours. Oxygen was produced by reacting 5 to 10 mg of samples with BrF₅ at 550°C for 8 to 12 hours. An internal standard (MQ quartz, δ¹⁸O = +10.1‰) was analyzed to calibrate the data to the V-SMOW scale. The mean values obtained from repeated analyses MQ gave a difference of 0.3 per mil from the accepted value. In the laser system oxygen was produced by heating quartz grains weighing typically 2 to 4 mg with a 40 W CO₂ laser in atmosphere of BrF₅. An internal standard (MONGT, δ¹⁸O = +5.55‰) was analyzed to calibrate the data to the V-SMOW scale. The technique of rapid heating using a defocused beam (Spicuzza et al., 1998) was used to minimize sample loss during the reaction, and yields were on average 92 percent of the expected amount for quartz. Duplicates gave agreement within 0.2 per mil. Hydrogen was produced by heating 10 to 30 mg of mineral concentrates in vacuum, following procedures described in Venemann and O'Neil (1993) and using a CuO furnace. Water was purified cryogenically and then reduced to H₂ by reaction with "Indiana Zinc" at 450°C, according to procedures adapted from Coleman et al. (1982). An internal silicate standard (AM muscovite, δD = -30‰) furnished a mean value of -30.5 per mil that was used to calibrate the data to the V-SMOW scale. Reproducibility is estimated to have been better than 4 per mil. Inclusion fluids (H₂O, CO₂) were liberated by decrepitation of fluid inclusions during heating of 1 to 2 g of quartz (fragments <3 mm) at temperatures >800°C. The quartz fragments were previously cleaned with HCl and HNO₃ and degassed at 200° and 300°C. The obtained water and CO₂ were trapped cryogenically and analyzed for hydrogen and carbon isotopes, respectively. Sulfur isotopes were analyzed in a Finnigan MAT 252 mass spectrometer at the Stable Isotope and ICP/MS Laboratory of the Queen's University, Kingston, Canada. For sulfur analysis, SO₂ was produced from 3 to 5 mg of pyrite loaded into tin capsules and reacted with CuO at 1,400°C in a He stream, using the Thermal Conversion/Elemental Analyzer-Isotope Ratio Mass Spectrometer technique. The analytical uncertainty for δ³⁴S was 0.5 per mil. The ¹³C/¹²C, ¹⁸O/¹⁶O, D/H, and ³⁴S/³²S ratios are reported in the delta notation, normalized to the PDB (carbon), V-SMOW (oxygen and hydrogen), and CDT (sulfur) scales.

Chlorite Geochemistry

The chlorite chemical composition was determined in a sample from the lower zone of the Chega Tudo deposit (Table 1). All the analyzed crystals are classified as daphnite (Fig. 7A) according to Hey (1954), with high iron content given by Fe/(Fe + Mg) ratios in the 0.80 to 0.85 range. The Al^{IV} values vary between 2.84 and 2.97 atoms per formula unit (a.p.f.u.), and the Ca + Na + K sum is always lower than 0.05 a.p.f.u. Despite the small variation, the Fe/(Fe+Mg) and Al^{IV} parameters show positive correlation (figure not included). These results, showing relatively homogeneous chemical composition, indicate that the chlorite attained chemical equilibrium with the hydrothermal fluid, but formation temperatures could not be calculated because the chlorite analyses plot below the Al saturation line on the Al-Mg-Fe plot (Fig. 7B), which makes them unsuitable for geothermometry (Cathelineau, 1988; Kranidiotis and MacLean, 1987).

TABLE 1. Chemical Composition of the Hydrothermal Chlorite from the Lower Level of the Mandiocal Orebody of the Chega Tudo Deposit

Analysis	82	83	84	86	88	90	92	93	99	100	101	103	104
SiO ₂ (wt %)	22.53	22.28	22.34	22.44	22.29	21.92	22.41	22.40	22.72	22.56	22.30	22.74	22.43
Al ₂ O ₃	20.91	21.40	20.75	21.41	21.66	20.62	21.48	21.21	21.11	20.94	21.33	21.62	21.45
FeO	39.18	38.16	38.67	39.74	39.95	40.48	40.38	40.33	38.49	38.37	39.36	39.05	39.13
MnO	0.54	0.55	0.52	0.53	0.46	0.53	0.57	0.52	0.42	0.53	0.48	0.44	0.46
MgO	5.44	4.99	5.13	4.13	4.39	4.24	3.99	4.20	5.33	5.30	4.64	4.88	4.48
CaO	<0.01	0.03	<0.01	0.03	0.02	0.03	0.03	<0.01	<0.01	0.05	0.02	0.05	0.06
Na ₂ O	0.02	<0.01	<0.01	<0.01	0.05	0.05	0.08	<0.01	0.02	<0.01	0.01	<0.01	0.04
K ₂ O	0.03	0.02	<0.01	0.01	<0.01	0.01	<0.01	0.02	0.03	0.01	0.02	0.04	0.06
H ₂ O	10.57	10.47	10.43	10.50	10.56	10.37	10.55	10.52	10.56	10.51	10.50	10.63	10.51
Total	98.65	97.43	97.41	98.29	98.82	97.88	98.94	98.68	98.12	97.76	98.16	98.82	98.11
Si	5.11	5.10	5.14	5.12	5.06	5.07	5.10	5.11	5.16	5.15	5.09	5.13	5.12
Al	5.59	5.77	5.62	5.76	5.79	5.62	5.75	5.70	5.65	5.63	5.74	5.75	5.76
Fe	7.43	7.31	7.43	7.59	7.59	7.83	7.68	7.69	7.31	7.33	7.52	7.37	7.47
Mn	0.10	0.11	0.10	0.10	0.09	0.10	0.11	0.10	0.08	0.10	0.09	0.08	0.09
Mg	1.84	1.70	1.76	1.41	1.49	1.46	1.35	1.43	1.80	1.80	1.58	1.64	1.52
Ca	0.00	0.01	0.00	0.01	0.01	0.01	0.01	0.00	0.00	0.01	0.01	0.01	0.02
Na	0.01	0.00	0.00	0.00	0.02	0.02	0.04	0.00	0.01	0.00	0.00	0.00	0.02
K	0.01	0.01	0.00	0.00	0.00	0.00	0.00	0.01	0.01	0.00	0.01	0.01	0.02
Al ^{IV}	2.888	2.898	2.864	2.876	2.938	2.928	2.903	2.890	2.840	2.850	2.907	2.869	2.882
Al ^{VI}	2.70	2.87	2.75	2.88	2.86	2.69	2.85	2.81	2.81	2.78	2.83	2.88	2.88
Fe/(Fe+Mg)	0.802	0.811	0.809	0.844	0.836	0.843	0.850	0.843	0.802	0.802	0.826	0.818	0.830
Si/Al	0.91	0.88	0.91	0.89	0.87	0.90	0.89	0.90	0.91	0.91	0.89	0.89	0.89
Ca+Na+K	0.02	0.01	0.00	0.01	0.03	0.03	0.04	0.01	0.02	0.02	0.02	0.02	0.05
Total cations	20.10	20.01	20.05	19.99	20.04	20.12	20.04	20.04	20.02	20.03	20.04	19.99	20.01



Fluid Inclusion Studies

The fluid inclusion study covers different vertical portions of the metavolcanic domain of the deposit. Analyses have been conducted on a gold-bearing, thick milky massive quartz vein from a surface exposure at Mina Velha and on gold-bearing quartz \pm calcite veinlets from the intermediate and lower mineralized zones at Mandiocal. Fifteen polished sections were examined under the microscope; of these, five that contained workable fluid inclusions were selected to carry out the microthermometric study. Over 200 inclusions were investigated by microthermometry, and the results are provided in a digital supplement to this paper at <http://www.geoscienceworld.org/> (or, for members and subscribers, on the SEG website, <http://www.segweb.org/>). Measurements were made of solid CO₂ melting temperature (T_{mCO_2}), clathrate melting temperature ($T_{mclathrate}$), CO₂ homogenization temperature (Th_{CO_2}), temperature of first observed melting (\sim eutectic) (Te), ice melting temperature (T_{mice}), total homogenization temperature (Th_L or V , where L stands for liquid and V for vapor). In addition, V_{CO_2} is the volumetric proportion of the carbonic phase (vol CO₂/vol total, in percentage), and V_g is the vapor volume (vol H₂O vapor/vol total, in percentage) in aqueous inclusions. Fluid compositions were calculated with the computer program

FIG. 7. A. Si versus Fe plot with the classification of chlorite from the Mandiocal orebody of the Chega Tudo deposit (a.p.f.u = atoms per formula unit). B. Ternary Al-Mg-Fe plot of the composition of the chlorite from the Mandiocal orebody of the Chega Tudo deposit. The dotted line is the boundary between Al-saturated (above) and Al-undersaturated (below) chlorites.

developed by Bakker (2003), using the appropriate equations of state for aqueous (Zhang and Frantz, 1987; Hall et al., 1988; Dubois and Marignac, 1997), aqueous-carbonic (Bowers and Helgeson, 1983; Duschek et al., 1990; Duan et al., 1992; Bakker, 1999), and carbonic fluid inclusions (Span and Wagner, 1996).

Fluid inclusion types and distribution

The studied fluid inclusions show a variety of shapes, including irregular, ovoid, and negative crystal forms, and their sizes vary between 5 and 12 μm , irrespective of the mineralized zone. Based on phase proportions at room and subzero temperatures, textural relationships, and microthermometric and microRaman results, five compositional types of fluid inclusions have been distinguished: (1) type 1: carbonic (rare, one-phase $\text{CO}_2\text{-CH}_4$ inclusions), (2) type 2a: aqueous-carbonic (abundant, two-phase $\text{CO}_2\text{-CH}_4\text{-H}_2\text{O-salt}$ inclusions), (3) type 2b: aqueous-carbonic (subordinate two-phase $\text{CO}_2\text{-H}_2\text{O-salt}$ inclusions), (4) type 3a: aqueous (abundant two-phase $\text{H}_2\text{O-NaCl-MgCl}_2$ inclusions), and (5) type 3b: aqueous (abundant two-phase $\text{H}_2\text{O-NaCl-KCl}$ inclusions).

In a thick vein from Mina Velha, medium- to coarse-grained quartz shows weakly to moderate undulose extinction. Fluid inclusions are randomly distributed or form large, three-dimensional arrangements (Fig. 8A). Only a few aqueous-carbonic inclusions of type 2b were identified with the CO_2 bubble occupying between 20 and 40 percent of the total volume.

The majority of the inclusions at Mina Velha are two-phase aqueous inclusions with a vapor bubble occupying <10 percent of the inclusion volume. Two petrographic subtypes have been distinguished (Table 2); type 3a are isolated and randomly distributed inclusions, whereas type 3b are secondary trail-bound inclusions.

The quartz vein from level 77m (intermediate zone) contains stringers of pyrite along fractures parallel to the foliation (Fig. 6C) as well as small euhedral to subhedral crystals of calcite. Large crystals of quartz are abundant and show variable effects of ductile deformation, such as subgrain development, deformation lamellae, and strong undulose extinction. However, some large crystals have been preserved from deformation and show straight extinction, allowing the fluid inclusion petrographic and microthermometric work to be done (Figs. 6H, 8 and 9). Fluid inclusions in these relics are distributed in several ways: in isolation, three-dimensional clusters, and planes (Fig. 8B, C) and intergranular contacts.

Both CO_2 -bearing and aqueous inclusions were identified in the intermediate zone. The CO_2 -bearing inclusions include subordinate one-phase carbonic (type 1) inclusions coexisting with two-phase aqueous-carbonic inclusions (type 2a). The type 2a are abundant inclusions and show variable phase proportions, but the CO_2 phase occupies 15 to 30 vol percent.

As in the surface vein, two populations of aqueous inclusions were also documented in the intermediate zone (Table 2). However, only a few individuals of the type 3a inclusions are spatially associated with the type 1 and 2a inclusions, and

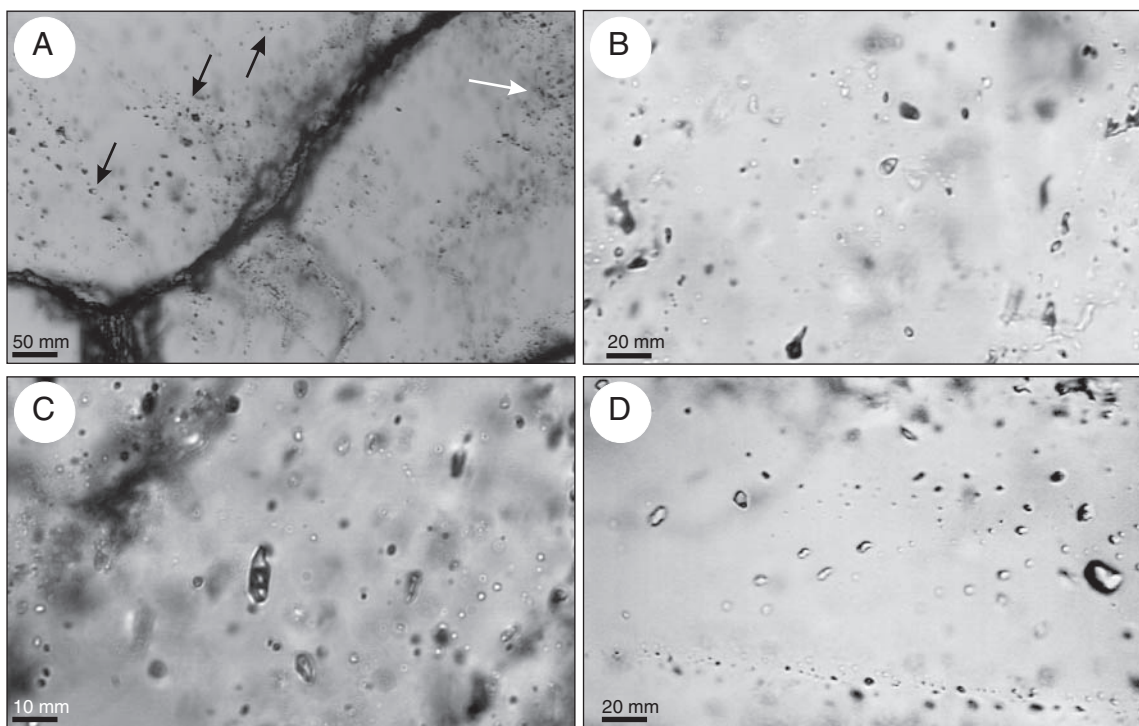


FIG. 8. Photomicrographs showing types and distribution of fluid inclusions in quartz from the Chega Tudo deposit. Photo A is from the Mina Velha vein and B to D photos are from the Mandiocall orebody. A. Discrete clusters of aqueous-carbonic fluid inclusions (black arrows) and aqueous inclusions distributed in clusters and trails (white arrow). B. Isolated carbonic and aqueous-carbonic inclusions. Note the trails in the left and right margins of the photograph with evidence of necking down. C. Random, three-dimensional distribution of aqueous-carbonic fluid inclusions. D. Random and trail-bound aqueous inclusions.

TABLE 2. Summary of the Microthermometric Data of Fluid Inclusions and Calculated Fluid Composition for Distinct Mineralized Orebodies and Vein Styles of the Chega Tudo Deposit

	Mina Velha		Mandiocal			
	Upper level		Intermediate level		Lower level	
Carbonic						
System	-		Type 1 CO ₂ -CH ₄		-	
Abundance	Absent		Rare		Absent	
Aqueous-carbonic						
System	Type 2b CO ₂ -H ₂ O-NaCl		Type 2a CO ₂ -CH ₄ -H ₂ O-NaCl		Type 2a (2b?) CO ₂ (± CH ₄)-H ₂ O-NaCl	
Abundance	Rare		Abundant		Subordinate	
V _{CO₂} %	20-40		15-30		15-30	
T _{mCO₂} (°C)	-56.6		-59.5 to -57.0		-57.6 to -56.6	
T _{mclathrate} (°C)	8.1-9.0		3.5-8.7		9.2-9.5	
wt % NaCl equiv	1.6-2.5		2.2-11.5		1.6	
Th _{CO₂} (°C)	13.4-14.0		9-17.9		14.0-15.0	
CO ₂ density g/cm ³	0.82-0.83		0.79-0.85		0.82-0.83	
bulk density g/cm ³	0.93-0.96		0.83-0.86		0.93-0.96	
X _{CO₂}	0.11-0.21		0.12-0.59		0.11-0.13	
X _{CH₄}	-		0.01-0.06		0-0.02	
X _{H₂O}	0.78-0.88		0.40-0.88		0.86	
X _{NaCl}	0.01		0.01-0.07		0.01	
Th (°C)	332-339		310-410		327-409	
Aqueous						
System	Type 3a NaCl-MgCl ₂	Type 3b NaCl-KCl	Type 3a NaCl-MgCl ₂	Type 3b NaCl-KCl	Type 3a NaCl-MgCl ₂	Type 3b NaCl-KCl
Abundance	Abundant	Abundant	Rare	Abundant	Rare	Abundant
V _g (%)	5-10	<5	15-20	<5	5-10	<5
Te (°C)	-34	-25	<-30	-22	<-34	-22 to -24
T _{mice} °C	-1.4 to -3.3	-0.1 to -2.6	-1.1 to -4.1	-2.1 to -8.5	-0.3 to -6.1	-0.3 to -7.6
Wt % NaCl equiv	2.5-5.5	0.2-4.2	2.0-6.7	3.4-12.3	0.5-9.3	0.5-11.2
Bulk density g/cm ³	0.63-0.88	0.89-0.96	0.54-0.68	0.89-1.02	0.78-0.87	0.93-1.00
Th (°C)	242-346	107-195	289-371	101-199	205-259	95-167

type 3b is texturally late with respect to the other types, occurring in sharp trails.

In the lower zone (levels 96m-96.5m), quartz occurs in millimeter-thick veinlets, with variable grain sizes, serrated to

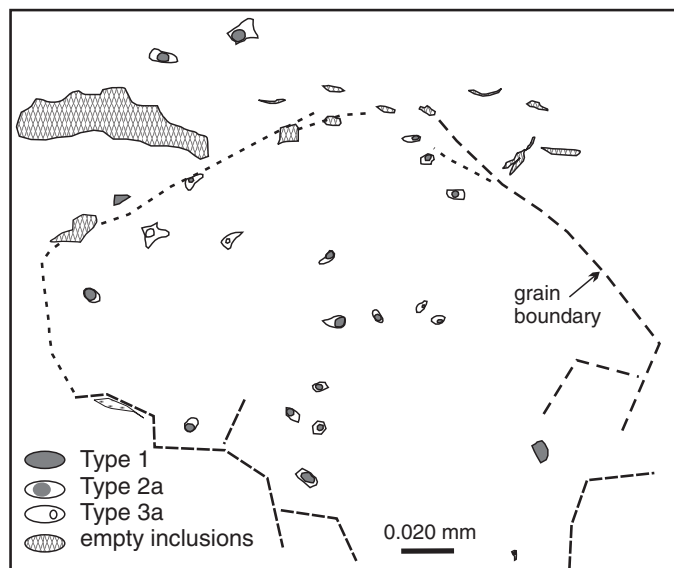


FIG. 9. Sketch showing the distribution and textural relationships between different fluid inclusion types in a single quartz crystal. Note the scarcity of inclusions and the presence of empty inclusions along grain boundaries. Sample from level 77m.

sharp contacts, weak to moderate undulose extinction, and minor subgrain development. The fluid inclusions are either randomly distributed or they occur in healed microfractures that are mainly orthogonal to the vein walls. Type 2a aqueous-carbonic inclusions are subordinate, being observed only in two clusters. Type 2a inclusions that have apparently not been affected by deformation have V_{CO₂} typically in the 15 to 30 percent range, but they are small (mostly <5 μm), which makes the observation of some phase changes difficult.

Type 3a aqueous inclusions are also very subordinate, having V_g of 5 to 10 vol percent. The predominant inclusions are aqueous type 3b inclusions with a small vapor phase (<5 vol %) that occurs either in trails or randomly distributed (Fig. 8D). In some samples they are the only type present.

We can not unequivocally relate any specific fluid inclusion type to gold mineralization, since we have not found gold particles in fluid inclusion cavities. However, the fluid inclusion study was performed in gold-bearing samples that are representative of the gold-quartz vein of Mina Velha (Fig. 4A) and gold-pyrite-quartz veinlet of the Mandiocal orebody (Fig. 6H). Therefore, we consider that the trapped fluids are representative of the evolution of the hydrothermal system (see below).

Microthermometry and Raman spectroscopic results

At Mina Velha, the melting of the solid CO₂ phase in type 2b inclusions was recorded at -56.6°C, indicating that the carbonic phase is composed of pure CO₂. The homogenization of the CO₂ into liquid occurred between 13.4° and 14.2°C. Two measurements of the clathrate melting were recorded at 8.1°

and 9.0°C, and the final homogenization into the liquid phase occurred between 332° and 339°C (Fig. 10).

Type 3a aqueous inclusions homogenize into liquid between 242° and 346°C, and the secondary type 3b inclusions homogenized between 107° and 195°C, also into liquid. Both subtypes have broadly the same range of ice-melting temperatures, from -1.4° to -3.4°C and -0.1° to -2.6°C, respectively (Fig. 10). However, ice first melting was observed at about -34°C in type 3a, and -25°C in type 3b, indicating distinct chemical systems for the two subtypes.

In the intermediate zone at Mandiocal, the T_{mCO_2} in both type 1 and 2a inclusions was recorded between -59.5° and -57.0°C (Fig. 10A), whereas T_{hCO_2} into liquid ranges from 9° to 17.9°C (Fig. 10B). Raman spectroscopic analysis confirmed that the carbonic phase is composed dominantly of CO_2 , with subordinate amounts of CH_4 (up to 10% of the volatile phase). Clathrates melted between 3.5° and 8.7°C, with a sharp mode at 7.4°C (Fig. 10C). A spread in the T_h data of these inclusions is observed, with homogenization occurring both to the liquid and gaseous phases, from 250° to 460°C. However, most of the values concentrate in the 310° to 410°C range, and a well-defined mode is observed at 355°C (Fig. 10D).

In type 3a inclusions, T_e is about -32°C, the vapor phase occupies 15 to 30 percent of the total volume, $T_{m_{ice}}$ is in the -1.1° to -4.1°C range, and the T_h into liquid varies from 289° to 371°C (Fig. 10D). Most of the aqueous inclusions, however, are texturally late type 3b inclusions. They have a small vapor bubble ($V_g < 5\%$), the eutectic melting temperature is about -22°C, $T_{m_{ice}}$ between -2.1° and -8.5°C, and the final homogenization into liquid occurred below 200°C.

In the lower zone at Mandiocal, the subordinate type 2a inclusions show T_{mCO_2} between -57.6° and -56.6°C, suggesting the large predominance of CO_2 in the carbonic phase. However, the small depression of T_{mCO_2} means that some CH_4 may also be present in the volatile phase. T_{hCO_2} was recorded at about 15°C into liquid. A few observed clathrates melted between 9.2° and 9.5°C. The final homogenization, mostly to the liquid phase, varies from 327° to 456°C, mainly between 327° and 340°C (Fig. 10). Inclusions with V_{CO_2} of 50 to 70 percent have the highest homogenization temperatures (>400°C). They are located close to necked inclusions and have probably been modified.

The few type 3a inclusions show $T_e < -34°C$, final ice melting from -0.3° to -6.1°C and $T_h(L) > 205°C$. Type 3b inclusions

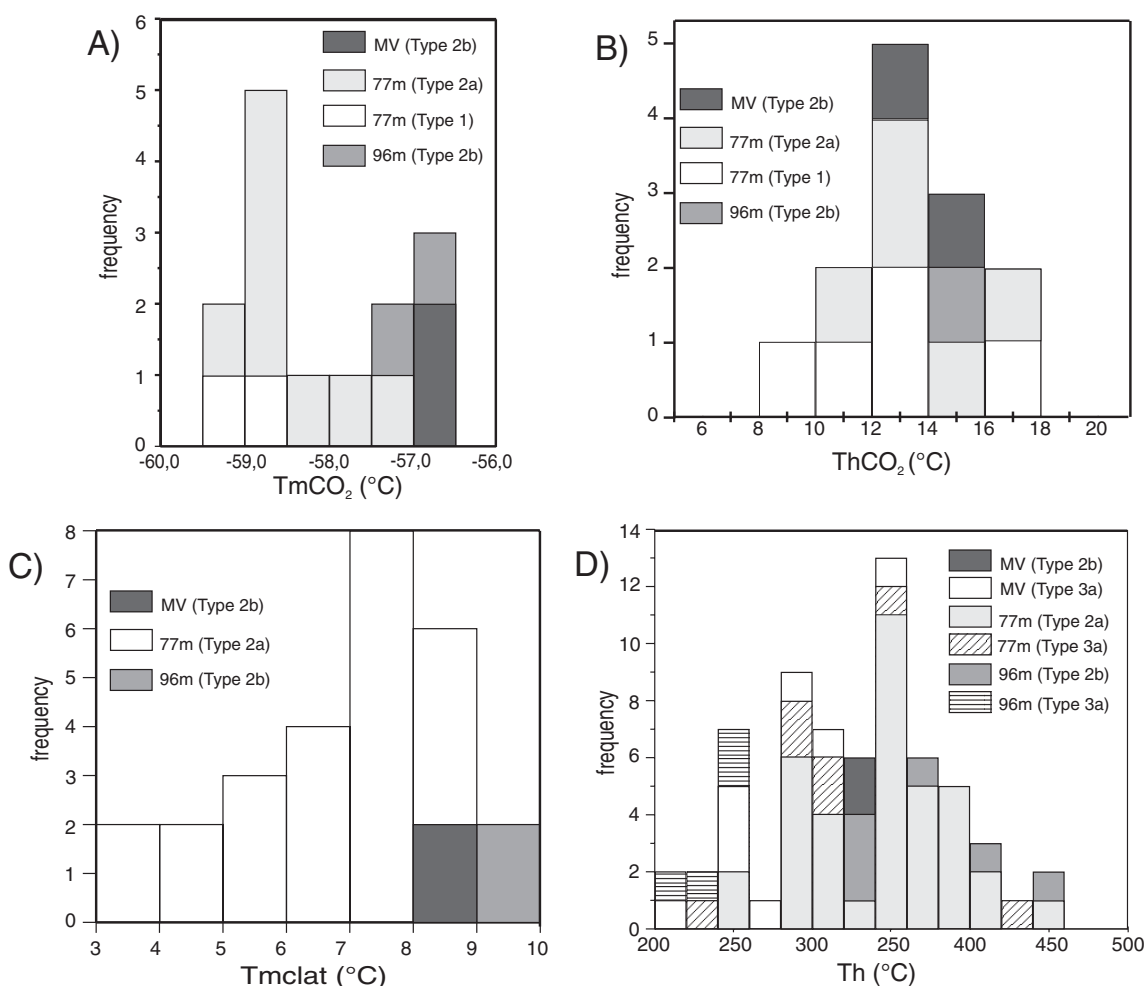


FIG. 10. Frequency histograms of microthermometric data for aqueous-carbonic and aqueous fluid inclusions of the Mina Velha and Mandiocal orebodies of the Chega Tudo deposit. A. CO_2 melting (T_{mCO_2}). B. Homogenization of CO_2 (T_{hCO_2}). C. Clathrate melting (T_{mclat}). D. Final homogenization (T_h).

show T_e between -22° and -24°C , final ice melting in the -0.3° to -7.6°C range, and final homogenization into liquid between 95° and 167°C .

Interpretation of Fluid Inclusion Data

Fluid inclusion populations, composition, and density

The five types of fluid inclusions recognized at Chega Tudo correspond to five compositional groups: (1) $\text{CO}_2\text{-CH}_4$ (type 1), (2) $\text{CO}_2\text{-CH}_4\text{-H}_2\text{O-NaCl}$ (type 2a), (3) $\text{CO}_2\text{-H}_2\text{O-NaCl}$ (type 2b), (4) $\text{H}_2\text{O-MgCl}_2$ (type 3a), and (5) $\text{H}_2\text{O-NaCl-KCl}$ (type 3b). These groups show some differences in their distribution, association, and composition within distinct mineralized zones, from surface down to 100 m in depth. A summary of the microthermometric results and calculated compositional data for each type is presented in Table 2.

The assemblage formed by types 2b and 3a occurs in the upper zone of the Mina Velha vein. Modeled in the $\text{CO}_2\text{-H}_2\text{O-NaCl}$ system (type 2b inclusions) this fluid is composed of 11 to 21 mol percent of CO_2 (mostly 11–13 mol %), 78 to 88 mol percent of H_2O , and has a salinity of 1.6 to 2.5 wt percent NaCl equiv. CO_2 density is 0.82 to 0.83 g/cm^3 , and the bulk density is between 0.93 and 0.96 g/cm^3 . The aqueous (Type 3a) inclusions have more variable salinity, between 2.0 and 6.7 weight percent NaCl equivalent. These aqueous inclusions contain other salt components in addition to, or instead of, NaCl, which may be MgCl_2 , as suggested by eutectic temperatures around -34°C (Crawford, 1981; Dubois and Marignac, 1997).

The types 1 and 2a fluid inclusions occur in close association, showing the same volatile composition and form a single fluid inclusion assemblage that is restricted to the intermediate zone of the Mandiocal orebody, and that may or may not be genetically associated with the few type 3a fluid inclusions. The composition of the fluid represented by these inclusions, modeled in the $\text{CO}_2\text{-CH}_4\text{-H}_2\text{O-NaCl}$ system, is 12 to 59 mol percent CO_2 (typically lower than 22 mol %), 1 to 6 mol percent CH_4 , 40 to 88 mol percent H_2O , and 1 to 7 mol percent NaCl (Table 2). A low salinity, averaging 5.8 ± 2.7 wt percent NaCl equiv, is estimated from $T_{m\text{clathrate}}$. Despite the presence of CH_4 , which might cause the underestimation of salinity (Collins, 1979), the low molar proportion of CH_4 suggests that the estimated values are a good approximation of the salinity of the fluid. The CO_2 density varies between 0.79 and 0.85 g/cm^3 , and the bulk density is moderate to high, in the range of 0.83 to 0.96 g/cm^3 .

This $\text{CO}_2\text{-CH}_4$ -bearing fluid also occurs in subordinate amounts in the lower zone, without the type 1 inclusions. However, it appears that the type 2a fluid in this zone is similar to the 2a and especially 2b types (Table 2), and probably were trapped at the same time.

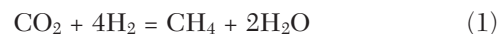
Type 3b inclusions are most likely composed of NaCl and KCl, as suggested by the eutectic melting temperatures of -22° and -25°C , respectively. This fluid was trapped late in the hydrothermal history of the deposit and will not be considered further.

Fluid behavior

When dealing with shear-zone hosted vein quartz gold deposits, it is always important to consider the role of postentrapment modifications on fluid inclusions (e.g., diffusion and

preferential removal of water induced by deformation: Hollister, 1990; Hall and Sterner, 1993; Huizenga and Touret, 1999). Relict crystals exhibiting minimal effects of strain and a reduced number of workable but apparently unmodified fluid inclusions were chosen for microthermometric measurements in order to minimize possible effects of such modifications. Nevertheless, postentrapment changes are still recognized in some investigated inclusions. For example, both the highest $\text{CO}_2(\pm\text{CH}_4)/\text{H}_2\text{O}$ ratios and final homogenization temperatures of some aqueous-carbonic inclusions ($>400^\circ\text{C}$), and the vertical trends in the T_h versus salinity plot (Fig. 11) may indicate partial leakage (e.g., Shepherd et al., 1985). The presence of dark, empty cavities close to grain boundaries in some microscopic domains (Fig. 9) may also indicate leakage during deformation.

However, the variation in the composition of the volatile phase, especially the CH_4 content, cannot be explained by postentrapment modification. The enrichment of the fluid in CH_4 could be caused by H_2 diffusion into the fluid inclusion, according to the reaction,



(Huizenga, 2001). This process could also explain some variation in the δD values of the fluids (see the Stable Isotopes section below), but it does not explain the variation in the oxygen isotope composition. We interpret that the variation in the composition of the volatile phase (and of the inclusion fluids as a whole) arises from the entrapment of distinct fluids or by the evolution of a single primary fluid.

A correlation between trapping temperatures and salinities (e.g., Cathelineau and Marignac, 1994) is expected if fluids having contrasting temperatures and/or salinities have mixed. Such relationship can be inferred for the aqueous-carbonic (type 2b) and the high-temperature aqueous (type 3a) inclusions present in samples from Mina Velha and the lower zone of Mandiocal (Fig. 11). In this case, the trend could indicate

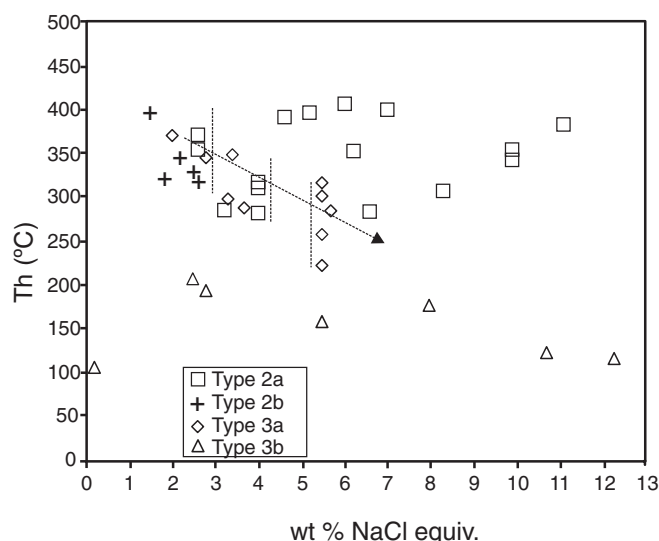


FIG. 11. Final homogenization (T_h) versus salinity (wt % NaCl equiv) diagram. Vertical dashed lines indicate possible leakage or trends for necking down trends.

mixing of a hotter and more dilute CO₂-bearing fluid with a colder and slightly more saline aqueous fluid.

During phase separation (fluid immiscibility) of a CO₂-CH₄-H₂O-salt fluid, the CH₄ content of the fluid decreases toward the end of the process in response to the higher gas distribution coefficient of the CH₄ compared to CO₂ (Drummond and Ohmoto, 1985). This may explain the CH₄-bearing type 2a fluid in deeper parts of the deposit.

At least some of the criteria used for the identification of fluid immiscibility (Ramboz et al., 1982; Frantz et al., 1992) are satisfied. These include (1) the contemporaneous entrapment of different fluid types, which is reflected in the co-existence of carbonic, aqueous-carbonic, and (subordinate) aqueous fluid inclusion in the intermediate zone, (2) homogenization of the inclusions both to the liquid and vapor phases over the same range of temperatures, (3) trapping of fluids in random proportions, which is observed to some extent, and (4) partitioning of salts into the aqueous-rich phase (Fig. 12A). A fluid with the composition as determined at Chega Tudo (XCO₂ < 22 mol %, ~5 wt % NaCl equiv) starts to unmix and enter the two-phase field at about 330° to 360°C

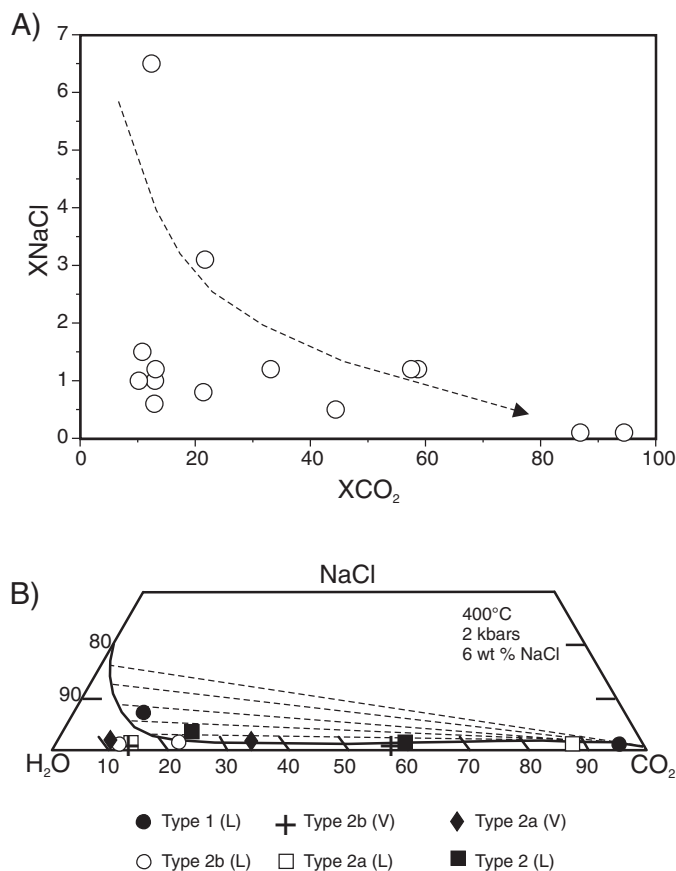


FIG. 12. Compositional relationships that may indicate fluid immiscibility. A. Calculated XCO₂ versus XNaCl plot for type 2a and 2b aqueous-carbonic fluid inclusions. The arrow indicates a possible trend of decreasing salinity as XCO₂ increases. B. Ternary diagram with the solvus for the CO₂-H₂O-NaCl system at 350°C, 2 kbars, and 6 wt percent NaCl equiv (after Bowers and Helgeson, 1983). Liquid and vapor fields are linked by dashed tie lines. The diagram shows pairs of type 2a and 2b fluid inclusions that homogenize to liquid (L) and vapor (V) in the same cluster or trail.

for pressures of 2 to 3 kbars (Bowers and Helgeson, 1983), which is in good agreement with the total homogenization temperatures of the fluid inclusions, and with the estimated trapping pressures (see below). Figure 12B shows that most of the fluid inclusion pairs plot on or near the solvus of the system in the two-phase immiscibility field, thus supporting the interpretation of fluid immiscibility occurring through phase separation from a homogeneous original fluid.

Another possibility for the presence of CH₄ at depth is the contamination of a primary aqueous-carbonic fluid through reaction with carbonaceous rocks that are part of the deposit stratigraphy, according to the hydrolysis reaction,



This process is supported by the strongly negative $\delta^{13}\text{C}$ values of the CO₂ trapped in the fluid inclusions of the intermediate zone (Table 3). Alternatively, a CH₄- or H₂-bearing fluid could have mixed with the CO₂.

In summary, the different fluid inclusion types trapped in quartz of the Chega Tudo deposit show complex compositional relationships that may be interpreted as having been produced by one or a combination of the following processes: (1) trapping of an evolving CO₂-CH₄-H₂O-NaCl fluid, with sporadic phase separation possibly affecting the CH₄/CO₂ ratio, (2) trapping of a CO₂-CH₄-H₂O-NaCl fluid and of a CO₂-H₂O-NaCl fluid in two discrete events or stages, also produced by immiscibility, (3) trapping of an immiscible CO₂-H₂O-NaCl fluid that acquired CH₄ through reaction with carbon-bearing host rocks, and (4) mixing of aqueous-carbonic and aqueous fluids. Irrespective of the process, fluid entrapment was accompanied by and/or followed by post-trapping modification.

Stable Isotopes

The results of stable isotope analyses are presented in Table 3. The quartz from mineralized veins has $\delta^{18}\text{O}$ values of 11.2 and 12.8 per mil in the Mina Velha vein, 14.2 per mil in the intermediate zone of Mandiocal, and +12.4 per mil in the lower zone of Mandiocal. In the barren alteration zone, the $\delta^{18}\text{O}$ value of quartz is +11.2 per mil. White mica has a $\delta^{18}\text{O}$ value of +9.4 at Mina Velha and +10.7 and +8.2 per mil in the intermediate and lower zones, respectively, at Mandiocal. The δD values of these white mica samples are -39, -49 and -50 per mil, respectively. The chlorite sample from the lower zone at Mandiocal has $\delta^{18}\text{O}$ value of +9.3 per mil and δD value of -62 per mil. The water extracted from fluid inclusions has a δD value of -12 per mil at Mina Velha and -37 and -26 per mil in the intermediate and lower zones, respectively, of the Mandiocal orebody. The $\delta^{13}\text{C}$ values of the CO₂ extracted from fluid inclusions are -6.9 per mil in the Mina Velha vein and -24.1 per mil in the intermediate zone of the Mandiocal orebody. The calcite sample from the intermediate zone has $\delta^{13}\text{C}$ and $\delta^{18}\text{O}$ values of -6.3 and +12.4 per mil, respectively. The pyrite from Mandiocal has a $\delta^{34}\text{S}$ value of 3.9 in a barren vein and values of 0.8 and 0.1 per mil in the intermediate and lower zones, respectively.

The oxygen isotope composition of the quartz is similar in Mina Velha and in the barren and lower zones of the Mandiocal orebody (11.2–12.8‰), but it is distinct in the intermediate zone of Mandiocal (14.2‰). This variation may imply that (1) fluids having different compositions but similar

TABLE 3. Stable Isotope Data from Alteration-Related Minerals from the Mina Velha and Mandiocal Orebodies of the Chega Tudo Gold Deposit

Sample no. and location	Mineral	Sampling site	Silicates		Carbonates		Fluid inclusions		Sulfides
			$\delta^{18}\text{O}$ (‰)	δD (‰)	$\delta^{13}\text{C}$ (‰)	$\delta^{18}\text{O}$ (‰)	$\delta^{13}\text{C}_{\text{CO}_2}$ (‰)	$\delta\text{D}_{\text{H}_2\text{O}}$ (‰)	$\delta^{34}\text{S}$ (‰)
Mina Velha (upper zone)									
MV/00	Quartz	Vein	+11.2				-6.9	-12	
11/00	Quartz	Vein	+12.8						
11/00	White mica	Vein	+9.4	-39					
Mandiocal (barren zone)									
16/69	Quartz	Alter zone	+11.2						
16/69	Pyrite	Alter zone							+3.9
Mandiocal (intermediate zone)									
16/77	Quartz	Veinlet	+14.2				-24.1	-37	
16/77	White mica	Veinlet	+10.7	-49					
16/77	Calcite	Veinlet			-6.3	+12.4			
16/77	Pyrite	Veinlet							+0.8
Mandiocal (lower zone)									
16/96	Quartz	Veinlet	+12.4				nd	-26	
16/96	White mica	Alter zone	+8.2	-50					
16/96	Chlorite	Alter zone	+9.3	-62					
16/96	Pyrite	Alter zone							+0.1

All analyses except for the barren sample 16/69 come from mineralized samples

*nd = not detected

temperature occurred in distinct zones, (2) quartz precipitated from a single fluid at different temperatures (cooling fluid), or (3) both fluid and temperature were variable in different zones. Similar variations are seen in the oxygen isotope composition of the white mica. However, the Δ values ($\Delta^{18}\text{O}_{\text{quartz-white mica}}$) in the three mineralized levels are nearly identical (Table 3), implying nearly the same temperature of formation for these two quartz-white mica pairs. The quartz-muscovite pairs yield temperatures of 370° and 360°C in Mina Velha and in the intermediate zone at Mandiocal, respectively, according to the geothermometer of Chacko et al. (1996). The higher Δ value in the lower zone at Mandiocal (4.2‰) indicates a lower temperature at this level (305°C). Alternatively, the quartz and white mica formed at different times within the paragenetic sequence, or isotope exchange occurred after mineral precipitation.

The quartz-chlorite pair of the lower zone at Mandiocal yielded temperatures of 611°C, according to the equation of Zheng (1993), and 508°C combining the fractionation factors of Matsuhisa et al. (1979) and Cole and Ripley (1999). These values are higher than the stability temperature of chlorite and indicate lack of equilibrium or incorrect fractionation factors. The quartz-calcite pair of the intermediate zone returned a temperature of 422°C according to the equation of Sharp and Kirchner (1994). However, an error of about $\pm 40^\circ\text{C}$ is associated with this temperature, since the quartz-calcite fractionation is not large.

The $\delta^{13}\text{C}$ from fluid inclusion CO_2 shows two contrasting values, -6.9 per mil at Mina Velha and -24.1 per mil in the intermediate zone at Mandiocal. The strongly negative value reflects the influence of organic carbon that most likely resulted from interaction between the fluid and reduced carbon

present in the carbonaceous schists that host part of the mineralization in the deepest metasedimentary domain of the deposit. Similar low $\delta^{13}\text{C}$ values have been found in graphite from schists in two other deposits of the Gurupi belt, Cachoeira and Serrinha (Klein et al., 2005a, 2006a). This is also consistent with the highest CH_4/CO_2 ratios recorded in fluid inclusions from the intermediate zone at Mandiocal that could result from fluid-rock reactions (reaction 2).

Fluid Evolution and Gold Mineralization

Consideration of the T - f_{O_2} - $p\text{H}$ and depth of ore deposition

The geologic information obtained in the Chega Tudo deposit, including the metamorphic grade of the host rocks, hydrothermal mineral assemblage, structural style, and temporal relationships between mineralization and metamorphism-deformation are consistent with ore formation at temperatures of 250° to 400°C (e.g., Mikucki and Ridley, 1993; Sibson, 2001). Fluid inclusion homogenization temperatures and equilibrium oxygen isotope relationships suggest that gold mineralization occurred at 330° to 370°C (Fig. 13), with different temperatures and/or stages in different domains of the deposit.

In the intermediate zone of the Mandiocal orebody, the fluid inclusion homogenization temperatures have a mode at 355°C, which is nearly identical to the temperature of 360°C obtained from the quartz-muscovite oxygen isotope thermometer. In the Mina Velha vein the quartz-muscovite pair yielded a temperature of 370°C, which is 30°C higher than the fluid inclusion homogenization temperatures, possibly indicating that the sampled quartz veins formed in different stages. In the lower zone at Mandiocal, the fluid inclusions

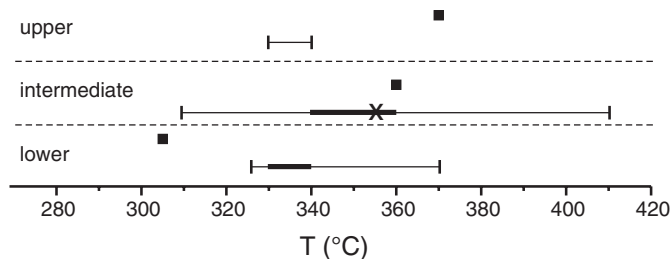


FIG. 13. Diagram showing the temperature variations obtained for distinct domains of the Chega Tudo deposit. The thin and thick bars represent the whole and main range of fluid inclusion homogenization temperatures; X indicates the modal value. Filled squares are temperatures obtained from oxygen isotope thermometry of the quartz-muscovite pair.

also reflect the lower temperature (330°–340°C). Assuming immiscibility, the homogenization temperatures represents the true trapping temperature and that no pressure correction is needed.

Oxygen fugacities have been calculated according to the method of Huizenga (2001), taking into account the main range of X_{CO_2} , the range of temperatures and an assumed pressure of 3 kbars, which is in keeping with the structural evidence, yielding $\log f_{O_2}$ values between -28.7 and -30.5 (340°–370°C) and -30.5 to -31.5 (330°–340°C) (Fig. 14A). The estimated T - f_{O_2} conditions plot within the pyrite and magnetite stability fields, above the CO_2 - CH_4 buffer and below the SO_2/H_2S buffer, indicating relatively reduced ore fluids. These conditions are consistent with the $\delta^{34}S$ values of

pyrite, the large predominance of CO_2 over CH_4 in fluid inclusions, and the absence of pyrrhotite and oxidized minerals, such as hematite and sulfates, in the alteration assemblage. The presence of white mica, absence of K-feldspar, and the stability of calcite imply near-neutral conditions with pH values between 5 and 6.2 (Fig. 14B).

Composition and sources of ore-forming fluid and solutes

The fluid inclusion study revealed two low-salinity (avg 2.0 and 5.8 wt % NaCl equiv) aqueous-carbonic fluids. The CO_2 content of the fluids is generally between 11 and 22 mol percent, and CH_4 is present in small amounts (<6 mol %) only in one type of fluid inclusion. Such fluids are consistent with a metamorphic origin (e.g., Phillips and Powell, 1993; McCuaig and Kerrich, 1998). We cannot unequivocally link these fluids to gold transport, but CO_2 -bearing fluids are the earliest fluids trapped in the fluid inclusions in each studied domain of the deposit and the CH_4 -bearing fluid is abundant in the intermediate zone, which has the highest gold grades. These fluids are interpreted to be representative of the ore-bearing fluids in the studied orebodies of the Chega Tudo deposit.

Using the estimated temperatures in Figure 13, the fluid $\delta^{18}O$ values were calculated by applying the quartz-water (Matsuhisa et al., 1979), muscovite-water (O'Neil and Taylor, 1969), chlorite-water (Cole and Ripley, 1999), and calcite-water (Friedman and O'Neil, 1977) fractionation factors. Fluid δD values were measured directly from inclusion fluids and calculated from the hydrous mineral data, using extrapolation of the chlorite-water (Graham et al., 1987) fractionation

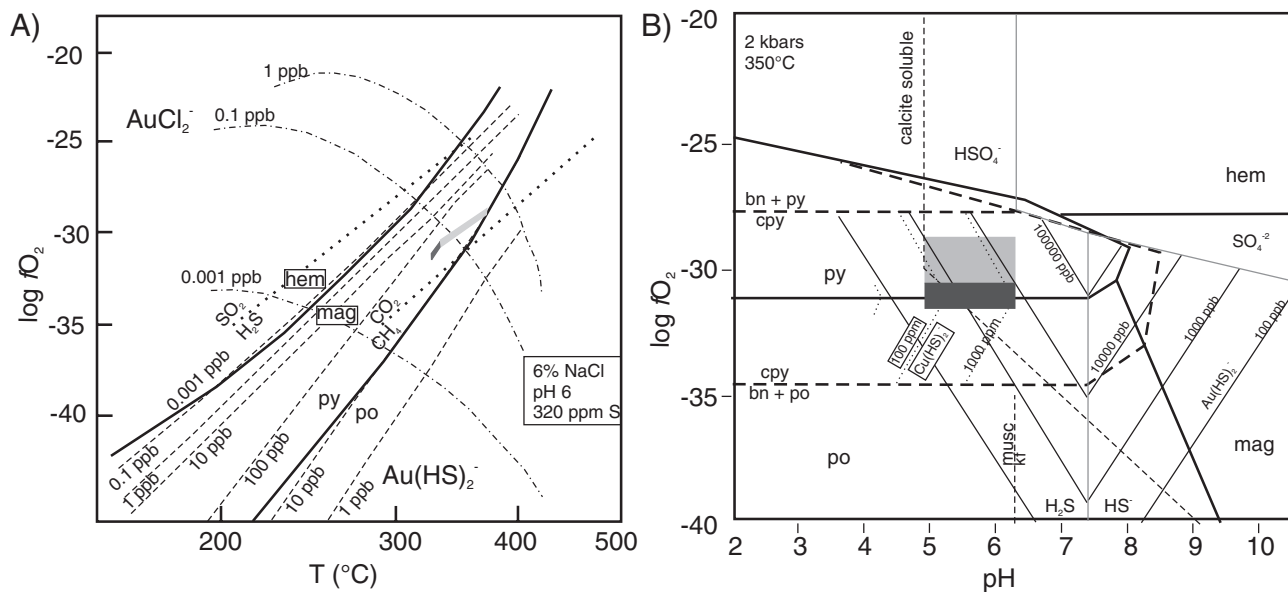


FIG. 14. A. Aqueous solubility of gold as a function of temperature and oxygen fugacity. Dashed lines are for the bisulfide complex $[Au(HS)_2^-]$, dotted-dashed lines are for the chloride complex $[AuCl_2^-]$. The heavy solid lines represent the limits of the stability fields of Fe-oxides and sulfides, and the dotted lines represent other buffers (adapted from Romberger, 1990, and Ohmoto and Goldhaber, 1997). B. Phase diagram showing the aqueous solubility of gold and chalcopyrite as bisulfide complexes ($Au(HS)_2^-$ and $Cu(HS)_2^-$, thin solid and dotted lines, respectively) as a function pH and oxygen fugacity at the temperature-pressure conditions estimated for the Chega Tudo deposit. Heavy solid and dashed lines show the stability fields of oxide and sulfide minerals; calculated according to Romberger (1990) and Wood (1998). In both diagrams the shaded areas represent the estimated physicochemical conditions for the Chega Tudo deposit. The light gray area is for the CO_2 - CH_4 - H_2O -NaCl fluid, and the dark gray field represents the CO_2 - H_2O -NaCl fluid; both correspond to conditions where gold and chalcopyrite are soluble. Mineral abbreviations: bn = bornite, cpy = chalcopyrite, hem = hematite, kf = K-feldspar, mag = magnetite, musc = muscovite, po = pyrrhotite, py = pyrite.

factor down to the estimated temperatures, and by applying the calibration of Bowers and Taylor (1985) for the muscovite-water fractionation. The $\delta^{13}\text{C}$ value of the fluid CO_2 was obtained directly by measuring the $\delta^{13}\text{C}$ of the CO_2 extracted from fluid inclusions, and by using the calcite- CO_2 equation for isotope fractionation of Ohmoto and Rye (1979). The $\delta^{34}\text{S}$ value of the fluid was calculated from the pyrite- H_2S fractionation factor of Ohmoto and Rye (1979), assuming H_2S as the main sulfur species in the fluid. The calculated compositions are presented in Table 4.

The full range of $\delta^{18}\text{O}_{\text{H}_2\text{O}}$ values is 5.3 to 9.7 per mil, but differences between different parts of the deposit (Fig. 15A) indicate fluid compositions consistent with the fluid inclusion results. The intermediate zone has the highest $\delta^{18}\text{O}_{\text{H}_2\text{O}}$ values ($>7.9\text{‰}$), whereas values lower than 7.2 per mil are restricted to the lower and upper zones. The $\delta^{18}\text{O}_{\text{H}_2\text{O}}$ values in equilibrium with chlorite are distinctly different from those of quartz and muscovite from the same level, supporting the interpretation that chlorite is not in equilibrium with the other two minerals. The δD values of water extracted from fluid inclusions are similar in the intermediate and lower zones (-37 and -29‰ , and -30 to -26‰ , respectively) but much higher in the upper zone (-12 to -19‰ at Mina Velha). The combined oxygen and hydrogen isotope data (Fig. 15B) are consistent with a metamorphic source for the fluids (e.g., produced by devolatilization and dehydration reactions during the prograde metamorphism of a volcanosedimentary sequence, at moderate depths in the crust: cf. Kerrick and Caldera, 1998; Yardley and Graham, 2002). This is consistent with the orogenic scenario proposed for the São Luís craton and Gurupi belt in the Paleoproterozoic (Klein et al., 2005b, c) (Fig. 16). Similar fluids could have been produced by syntectonic muscovite-bearing granitoids, followed by dilution by other fluid types (metamorphic, meteoric). The subtle trend in the $\delta^{18}\text{O}$ versus δD plot (Fig. 15B), showing decreasing $\delta^{18}\text{O}$ and increasing δD values from the intermediate to the two other

levels, is consistent with the higher temperature of ore deposition in the intermediate zone. However, we cannot discount minor influx of meteoric water into the system (type 3a fluid inclusions?), possibly in the lower zone which has isotopic values between those found in the upper and intermediate zones.

The strongly negative $\delta^{13}\text{C}$ value of inclusion CO_2 (-24.1‰) comes from organic contribution. The value of -6.9 per mil overlaps the compositional fields of mantle-, magmatic-, and metamorphic-derived carbon, as well as of mixed crustal sources (Ohmoto, 1986; McCuaig and Kerrich, 1998). The fluid $\delta^{13}\text{C}$ values calculated from the calcite- CO_2 fractionation are -3.8 to -3.9 per mil and could represent a distinct carbon source, possibly a crustal source. It is likely that the calcite did not precipitate from the same CO_2 found in the inclusions, and this may explain the lack of equilibrium between quartz and calcite in this part of the deposit.

The $\delta^{34}\text{S}$ values of H_2S in the mineralized zones range from -0.2 to -1.0 per mil and indicate a reduced character for the ore fluid (below the $\text{SO}_2/\text{H}_2\text{S}$ boundary: Fig. 14) and consistent with the fluid inclusion evidence. These values also are consistent with an igneous source of sulfur (Lambert et al., 1984; Kerrich, 1987).

Gold transport and deposition

At the estimated T- f_{O_2} -pH conditions, H_2S is the predominant sulfur species in the fluid (Fig. 14) and AuHS_2^- is likely to have been the dominant gold-transporting complex (Hayashi and Ohmoto, 1991; Benning and Seward, 1996). These conditions are also consistent with high solubility of gold and copper as bisulfide complexes (Fig. 14), which may explain the association of gold and chalcopyrite in the veins. The different styles of gold mineralization at Mina Velha (free-milling gold) and Mandiocal (refractory and free gold) could indicate different mechanisms for gold precipitation, differences in the extent of fluid-wall rock interaction, or two separate mineralization events from distinct ore fluids.

The fluid inclusion study indicates that fluid immiscibility and mixing were possible causes of gold deposition. Although fluid immiscibility has been documented at both Mina Velha and Mandiocal, the following all indicate changing redox and pH of the fluid, which also may have contributed to gold precipitation: (1) relatively large volume of altered wall rock, (2) sulfidation of the host rocks (reaction between sulfur and iron-rich minerals, such as magnetite, early pyrite and chlorite), (3) the presence of gold in fractures of pyrite, and (4) the low $\delta^{13}\text{C}$ values of fluid inclusion CO_2 .

Concluding Remarks: A Fluid-Structural Model

The Chega Tudo gold deposit is associated with the major strike-slip Tentugal shear zone located at the boundary between the São Luís craton and the Gurupi belt. The orebodies are hosted in 2160 to 2148 Ma greenschist facies volcanosedimentary rocks, and are parallel to the subvertical structural grain. The hydrothermal alteration associated with the gold mineralization includes silicification, chloritization, carbonatization, sericitization, and sulfidation of the host rocks. Alteration occurred at high fluid-to-rock ratios as suggested by extensive quartz \pm carbonate veining and the minimal variation in the fluid isotope compositions within the

TABLE 4. Calculated Stable Isotope Compositions for Fluids in Equilibrium with Minerals of the Mina Velha and Mandiocal Orebodies of the Chega Tudo Gold Deposit

Sample/ level	Mineral	$\delta^{18}\text{O}_{\text{H}_2\text{O}}$ (‰)	$\delta\text{D}_{\text{H}_2\text{O}}$ (‰)	$\delta^{13}\text{C}_{\text{CO}_2}$ (‰)	$\delta^{34}\text{S}_{\text{H}_2\text{S}}$ (‰)
Mina Velha upper zone (T = 330–340°C)					
MV/00	Quartz	+5.3 to +6.4	-12 ¹	-6.9 ¹	
11/00	Quartz	+6.9 to +7.2			
11/00	White mica	+6.7 to +7.0	-19		
Mandiocal intermediate zone (T = 340–370°C)					
16/77	Quartz	+8.6 to +9.4	-37 ¹	-24.1 ¹	
16/77	White mica	+8.3 to +8.8	-29		
16/77	Calcite	+7.9 to +8.6		-3.8 to -3.9	
16/77	Pyrite				-0.2 to -0.3
Mandiocal lower zone (T = 330–340°C)					
16/96	Quartz	+6.5 to +6.8	-26 ¹		
16/96	White mica	+5.5 to +6.3	-30		
16/96	Chlorite	+9.6 to +9.7	-28		
16/96	Pyrite				-1.0

¹ Fluid inclusion water and CO_2

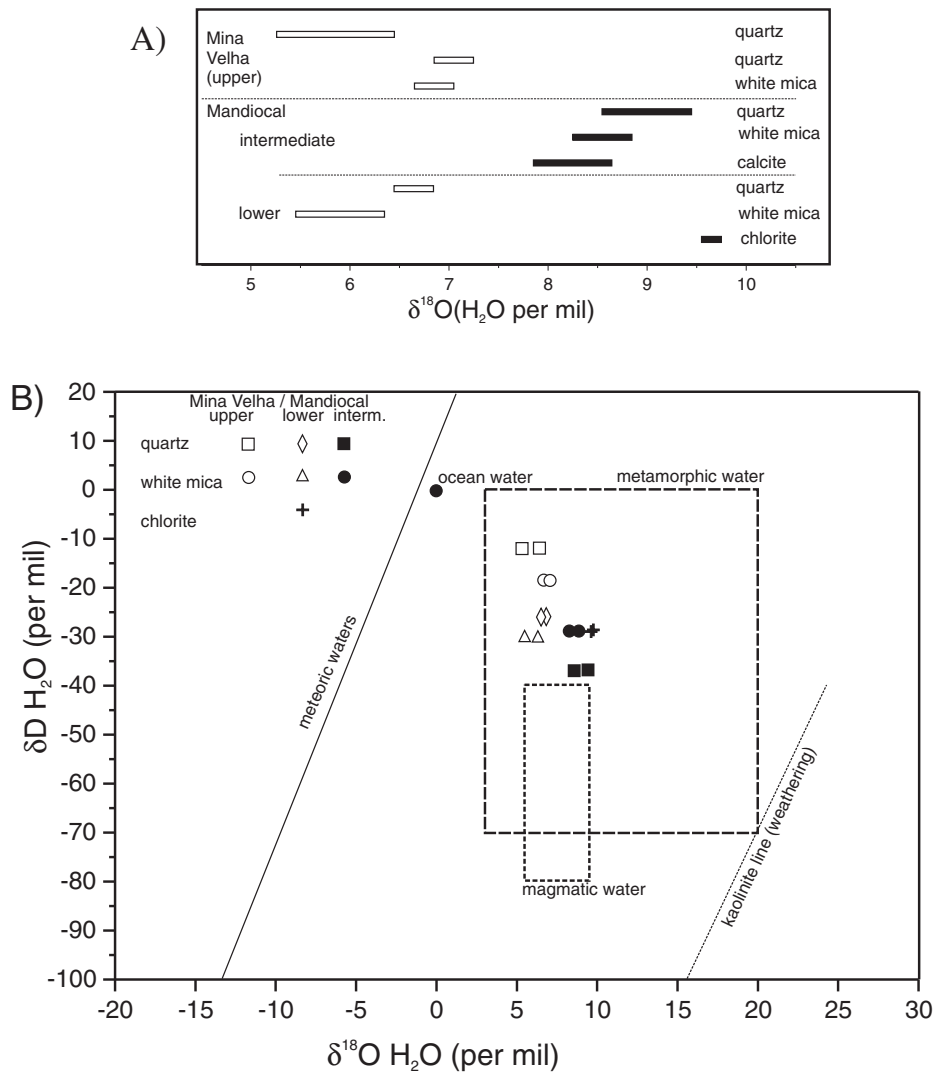


FIG. 15. Calculated oxygen and hydrogen isotope compositions of water from analyses of hydrothermal mineral and inclusion fluids from the Mina Velha and Mandiocal orebodies of the Chega Tudo deposit. Fields of magmatic and metamorphic waters in B are those defined by Sheppard (1986).

alteration zones. Preliminary evidence suggests a Paleoproterozoic age (2060–2000 Ma) for mineralization, at the end of a protracted regional orogenic evolution.

Integrated structural, mineralogical, fluid inclusion, and stable isotope data suggest that deposition of auriferous quartz veins and stringers of auriferous pyrite occurred in dilatational sites (fractures, foliation openings, vein-wall rock contacts) under fluctuating pressure conditions. The data also indicate that mineralization at Chega Tudo occurred in response to complex and concurrent processes involving fluid immiscibility, fluid-rock reactions, and possibly fluid mixing. Gold mineralization in the intermediate zone of the Mandiocal orebody and at Mina Velha formed from slightly different ore fluids. The main differences are the abundance of CO_2 -bearing inclusions, the presence of CH_4 , and higher salinities in the intermediate zone, the $\delta^{18}\text{O}$, δD , and $\delta^{13}\text{C}$ values of the fluids, and the calculated f_{O_2} values. The lower zone at Mandiocal records, at least in part, the two stages of mineralization.

A reasonable interpretation that might explain the different physicochemical characteristics of the fluids and the two styles of gold mineralization involves (1) a deeply sourced, low-salinity CO_2 - H_2O - NaCl -bearing metamorphic fluid that migrated through active structures related to the Tentugal shear zone under fluctuating pressure conditions (e.g., McCuaig and Kerrich, 1998; Sibson, 2001), (2) hydrothermal alteration of the enclosing rocks and vein precipitation at high fluid pressures, (3) enrichment of this fluid in CH_4 through interaction with C-bearing rocks in the proximity of the deposit, and (4) a sudden drop in the fluid pressure caused fluid immiscibility forcing the fluid back into the shear zone (e.g., Cox et al., 1995) where it mixed with a deeply sourced CO_2 - H_2O - NaCl fluid and a H_2O - NaCl - MgCl_2 fluid of metamorphic (\pm metamorphic?) origin or exchanged with metamorphic rocks (Figs. 17). The two parts of Chega Tudo have characteristics that are analogous to those of orogenic gold deposits hosted in metamorphic belts elsewhere (Groves et al., 1998;

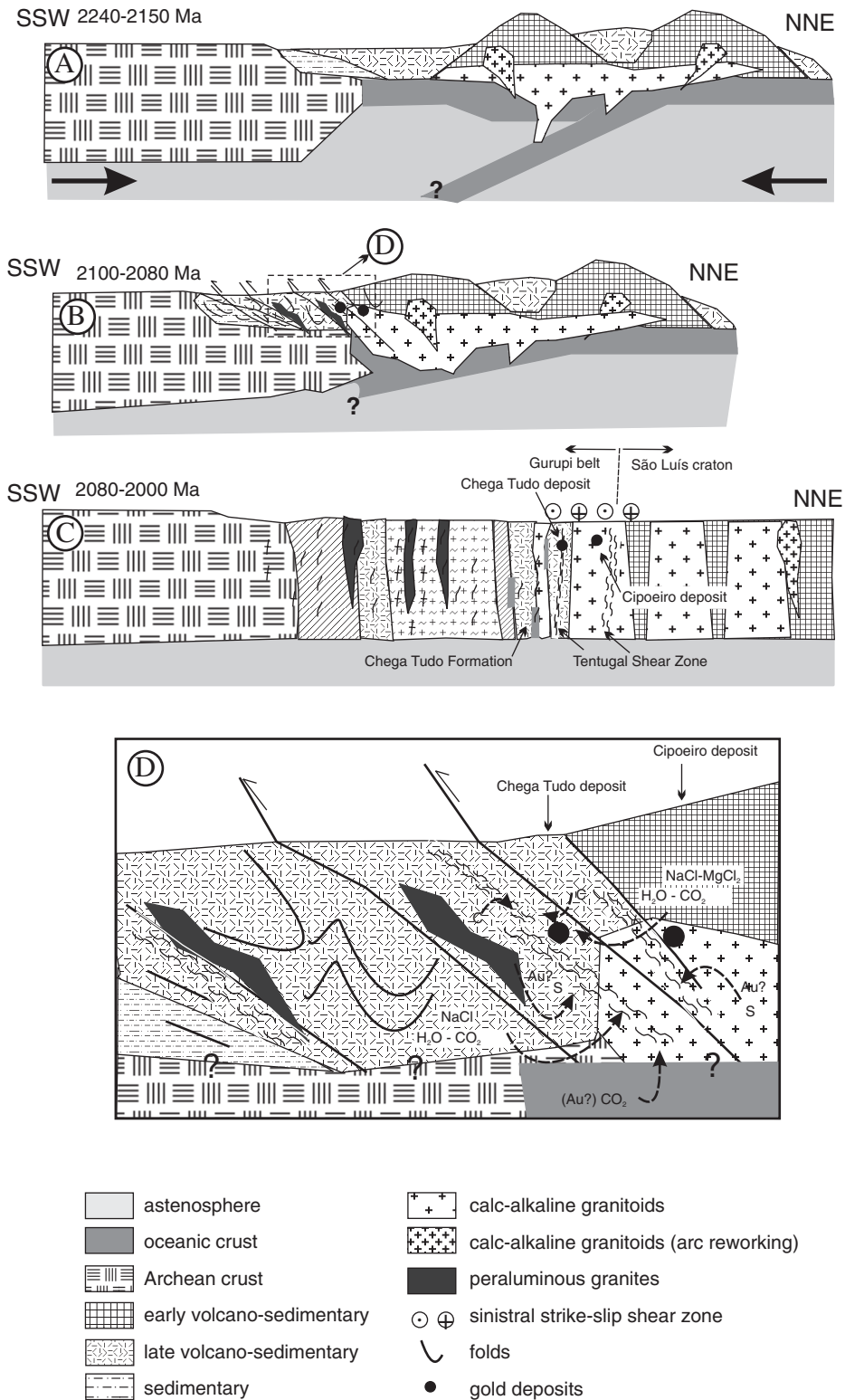


FIG. 16. Schematic (not to scale) cross sections illustrating the Paleoproterozoic geodynamic evolution of the Gurupi belt and São Luís craton. A. Accretion phase: intra-oceanic arc construction, subduction, calc-alkaline magmatism, and concomitant reworking of the island arc. B. Collision phase: accretion of juvenile terranes to an Archean block, moderate crust thickening, metamorphism, crustal melting and peraluminous magmatism. C. Strike-slip shearing, parallelism of units, and gold mineralization (modified from Klein et al., 2005b). D. Detail of the mineralized portion of the Gurupi belt showing the position of the Chega Tudo and Cipoeiro gold deposits and possible fluid and solute sources and paths.

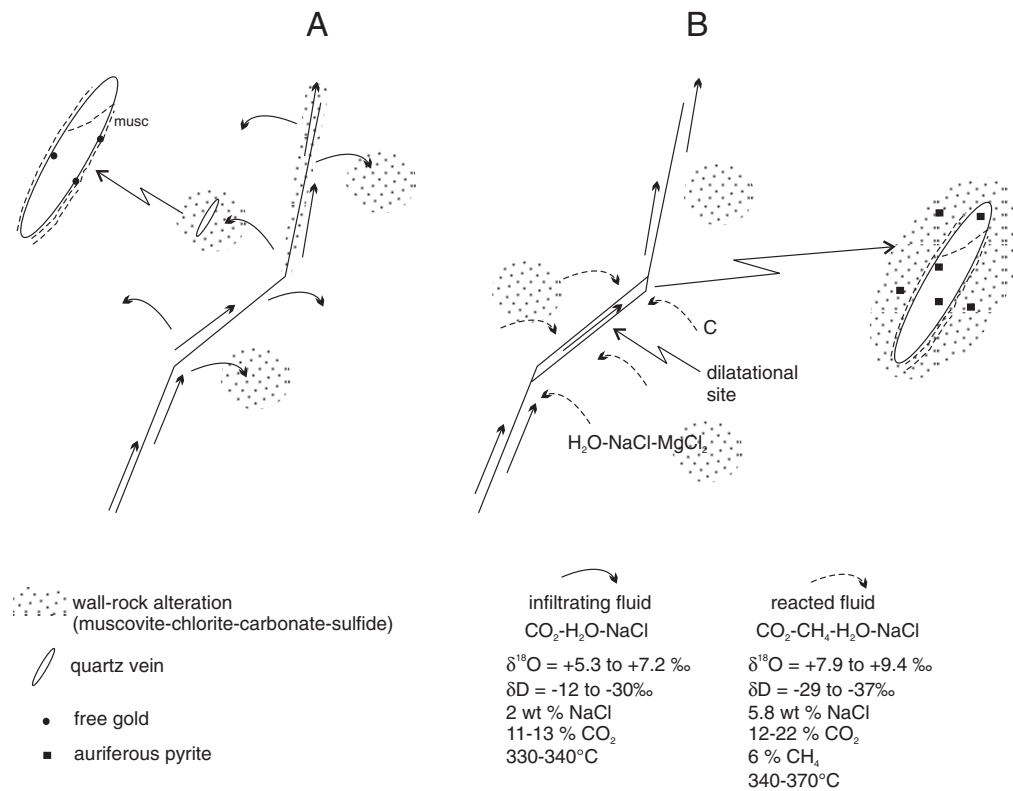


FIG. 17. Schematic (not to scale) illustration of possible mechanisms of fluid migration responsible for the Chega Tudo gold deposit (based on Cox et al., 1995). A. Prefault failure with upward and outward migration of a deeply sourced fluid, wall-rock alteration, vein formation, and deposition of free gold. B. Immediate postfault failure with upward migration of the deeply sourced fluid and backward migration of the reacted fluid, with vein formation and precipitation of refractory gold.

McCuaig and Kerrich, 1998; Goldfarb et al., 2005) and likely formed in a similar manner.

Acknowledgments

This study benefited from financial support provided by CAPES (BEX 2020/02-05), CPRM/Geological Survey of Brazil, and UFPA. The senior author acknowledges the Brazilian agency Conselho Nacional de Desenvolvimento Científico e Tecnológico (CNPq) for a research grant (process 308994/2006-0). C. Torresini, G.M. Brandão, and S.J.C. Melo are gratefully acknowledged for field support and discussions on the geology of the deposit. R. Angélica (UFPA), C. Lamarão (UFPA), and K. Fuzikawa (CDTN/CNEN), kindly helped with the XRD, SEM, and Raman analyses, respectively. Assistance and discussions with C. Renac (Université Jean Monnet) were greatly appreciated. Steffen Hagemann is thanked for the suggestions made on an earlier version of the manuscript, which also benefited from valuable and incisive comments and suggestions of the two *Economic Geology* reviewers (Robert Kerrich and Peter Neumayr) and from the editorial handling of Mark Hannington.

July 3, 2007; June 3, 2008

REFERENCES

- Almeida, F.F.M., Melcher, G.C., Cordani, U.G., Kawashita, K., and Vandomos P., 1968, Radiometric age determinations from northern Brazil: *Boletim da Sociedade Brasileira de Geologia*, v. 17, p. 3–14.
- Araujo Neto, H., 1998, Programa Nacional de Prospecção de Ouro – PNPO. Mapa de reservas e produção de ouro do Brasil. Brasília, Companhia de Pesquisa de Recursos Minerais, scale 1:7.000.000.
- Bakker, R.J., 1999, Adaptation of the Bowers and Helgeson (1983) equation of state to the $\text{H}_2\text{O-CO}_2\text{-CH}_4\text{-N}_2\text{-NaCl}$ system: *Chemical Geology*, v. 154, p. 225–236.
- 2003, Package FLUIDS 1. Computer programs for analysis of fluid inclusion data and for modelling bulk fluid properties: *Chemical Geology*, v. 194, p. 3–23.
- Benning, L.G., and Seward, T.M., 1996, Hydrosulphide complexing of Au(I) in hydrothermal solutions from 150 to 400°C and 500 to 1500 bars: *Geochimica et Cosmochimica Acta*, v. 60, p. 1849–1871.
- Bowers, T.S., and Helgeson, H.C., 1983, Calculation of the thermodynamic and geochemical consequences of nonideal mixing in the system $\text{H}_2\text{O-CO}_2\text{-NaCl}$ on phase relations in geological systems: Equation of state for $\text{H}_2\text{O-CO}_2\text{-NaCl}$ fluids at high pressures and temperatures: *Geochimica et Cosmochimica Acta*, v. 47, p. 1247–1275.
- Bowers, T.S., and Taylor, Jr., H.P., 1985, An integrated chemical and stable-isotope model of the origin of midocean ridge hot spring systems: *Journal of Geophysical Research*, v. 90, p. 12,583–12,606.
- Cathelineau, M., 1988, Cation site occupancy in chlorites and illites as a function of temperature: *Clay Minerals*, v. 23, p. 471–485.
- Cathelineau, M., and Marignac, C., 1994, Use of fluid inclusions for a better understanding of intracontinental geothermal activities, in De Vivo, B., and Frezzotti, M.L., eds., *Fluid inclusions in minerals: Methods and applications*: Blacksburg, Virginia Polytechnic Institute and State University, p. 309–326.
- Chacko, T., Hu, X., Mayeda, T.K., Clayton, R.N., and Goldsmith, J.R., 1996, Oxygen isotope fractionations in muscovite, phlogopite, and rutile: *Geochimica et Cosmochimica Acta*, v. 60, p. 2595–2608.
- Clayton, R.N., and Mayeda, T.K., 1963, The use of bromine pentafluoride in the extraction of oxygen from oxides and silicates from isotopic analyses: *Geochimica et Cosmochimica Acta*, v. 27, p. 43–52.

- Cole, D.R., and Ripley, E.M., 1999, Oxygen isotope fractionation between chlorite and water from 170 to 350°C: A preliminary assessment on partial exchange and fluid/rock experiments: *Geochimica et Cosmochimica Acta*, v. 63, p. 449–457.
- Coleman, M.L., Shepherd, T.J., Durham, J.J., Rouse, J.E., and Moore, G.R., 1982, Reduction of water with zinc for hydrogen isotope analysis: *Analytical Chemistry*, v. 54, p. 993–995.
- Collins, P.L.F., 1979, Gas hydrates in CO₂-bearing fluid inclusions and the use of freezing data for estimation of salinity: *ECONOMIC GEOLOGY*, v. 74, p. 143–1444.
- Costa, J.B.S., Pastana, J.M.N., Costa, E.J.S., and Jorge-João, X.S., 1988, A faixa de cisalhamento Tentugal na Folha SA.23-Y-B: Congresso Brasileiro de Geologia, 35th, Belém, Anals, v. 5, p. 2257–2266.
- Costa, J.L., 2000, Programa Levantamentos Geológicos Básicos do Brasil, Programa Grande Carajás: Castanhal, Folha SA.23-V-C. Estado do Pará. Belém, Companhia de Pesquisa de Recursos Minerais (on CD-ROM).
- Cox, S.F., Sun, S.S., Etheridge, M.A., Wall, V.J., and Potter, T.F., 1995, Structural and geochemical controls on the development of turbidite-hosted gold quartz vein deposits, Wattle Gully mine, Central Victoria, Australia: *ECONOMIC GEOLOGY*, v. 90, p. 1722–1746.
- Crawford, M.L., 1981, Phase equilibria in aqueous fluid inclusions, in Hollister, L.S., and Crawford, M.L., eds., *Fluid inclusions: Applications in petrology*: Mineralogical Association of Canada, Short Course Handbook, v. 6, p. 75–100.
- Drummond, S.E., and Ohmoto, H., 1985, Chemical evolution and mineral deposition in boiling hydrothermal systems: *ECONOMIC GEOLOGY*, v. 80, p. 126–147.
- Duan, Z., Möller, N., and Weare, J.H., 1992, An equation of state for the CH₄-CO₂-H₂O system: II. Mixtures from 50 to 1000 °C and 0 to 1000 bar: *Geochimica et Cosmochimica Acta*, v. 56, p. 2619–2631.
- Dubois, M., and Marignac, C., 1997, The H₂O-NaCl-MgCl₂ ternary phase diagram with special application to fluid inclusion studies: *ECONOMIC GEOLOGY*, v. 92, p. 114–119.
- Duschek, W., Kleinrahm, R., and Wagner, W., 1990, Measurements and correlation of the (pressure, density, temperature) relation of carbon dioxide: II. Saturated-liquid and saturated-vapour densities and the vapour pressure along the entire coexistence curve: *Journal of Chemical Thermodynamics*, v. 22, p. 841–864.
- Frantz, J.D., Popp, R.K., and Hoering, T.C., 1992, The compositional limits of fluid immiscibility in the system H₂O-NaCl-CO₂ as determined with the use of synthetic fluid inclusions in conjunction with mass spectrometry: *Chemical Geology*, v. 98, p. 237–255.
- Friedman, I., and O'Neil, J.R., 1977, Compilation of stable isotope fractionation factors of geochemical interest: U.S. Geological Survey Professional Paper, v. 440-KK, p. 1–12.
- Goldfarb, R.J., Baker, T., Dubé, B., Groves, D.I., Hart, C.J.R., and Gosselin, P., 2005, Distribution, character, and genesis of gold deposits in metamorphic terranes: *ECONOMIC GEOLOGY 100TH ANNIVERSARY VOLUME*, p. 407–450.
- Graham, C.M., Viglino, J.A., and Harmon, R.S., 1987, Experimental study of hydrogen-isotope exchange between aluminous chlorite and water and of hydrogen diffusion in chlorite: *American Mineralogist*, v. 72, p. 566–579.
- Groves, D.I., Goldfarb, R.J., Gebre-Mariam, M., Hagemann, S.G., and Robert, F., 1998, Orogenic gold deposits: A proposed classification in the context of their crustal distribution and relationships to other gold deposit types: *Ore Geology Reviews*, v. 13, p. 7–27.
- Hall, D.L., and Sterner, S.M., 1993, Preferential water loss from synthetic fluid inclusions: *Contributions to Mineralogy and Petrology*, v. 114, p. 489–500.
- Hall, D.L., Sterner, S.M., Bodnar, R.J., 1988, Freezing point depression of NaCl-KCl-H₂O solutions: *ECONOMIC GEOLOGY*, v. 83, p. 197–202.
- Harris, C., Stuart Smith, H., and le Roex, A.P., 2000, Oxygen isotope composition of phenocrysts from Tristan da Cunha and Gough island lavas: Variation with fractional crystallization and evidence for assimilation: *Contributions to Mineralogy and Petrology*, v. 138, p. 164–175.
- Hayashi, K.I., and Ohmoto, H., 1991, Solubility of gold in NaCl- and H₂S-bearing aqueous solutions at 250–350°C: *Geochimica et Cosmochimica Acta*, v. 55, p. 2111–2126.
- Hey, M. H., 1954, A new review of the chlorites: *Mineralogical Magazine*, v. 30, p. 277–292.
- Hodgson, C.J., 1989, The structure of shear-related, vein-type gold deposits: A review: *Ore Geology Reviews*, v. 4, p. 231–273.
- Hollister, L.S., 1990, Enrichment of CO₂ in fluid inclusions in quartz by removal of H₂O during crystal-plastic deformation: *Journal of Structural Geology*, v. 12, p. 895–901.
- Huizenga, J.M., 2001, Thermodynamic modeling of C-O-H fluids: *Lithos*, v. 55, p. 101–114.
- Huizenga, J.M., and Touret, J.L.R., 1999, Fluid inclusions in shear zones, the case of the Umwindi shear zone in the Harare-Shamva-Bindura greenstone belt, NE Zimbabwe: *European Journal of Mineralogy*, v. 11, p. 1079–1090.
- Kerrick, R., 1987, The stable isotope geochemistry of Au-Ag vein deposits in metamorphic rocks, in Kyser, T.K., ed., *Stable isotope geochemistry of low temperature fluids*: Mineralogical Association of Canada, Short Course Handbook, v. 13, p. 287–336.
- Kerrick, D.M., and Caldera, K., 1998, Metamorphic CO₂ degassing from orogenic belts: *Chemical Geology*, v. 145, p. 213–232.
- Klein, E.L., and Moura, C.A.V., 2001, Age constraints on granitoids and metavolcanic rocks of the São Luís craton and Gurupi belt, northern Brazil: Implications for lithostratigraphy and geological evolution: *International Geology Review*, v. 43, p. 237–253.
- 2008, São Luís craton and Gurupi belt (Brazil): Possible links with the West-African craton and surrounding Pan-African belts, in Pankhurst, R.J., Trouw, R.A.J., Brito Neves, B.B., and de Wit, M.J., eds., *West Gondwana: Pre-Cenozoic correlations across the South Atlantic region*: Geological Society, London, Special Publications, v. 294, p. 137–151.
- Klein, E.L., Harris, C., Giret, A., Moura, C.A.V., and Angélica, R.S., 2005a, Geology and stable isotope (O, H, C, S) constraints on the genesis of the Cachoeira gold deposit, Gurupi belt, northern Brazil: *Chemical Geology*, v. 221, p. 188–206.
- Klein, E.L., Moura, C.A.V., Krymsky, R., and Griffin, W.L., 2005b, The Gurupi belt in northern Brazil: Lithostratigraphy, geochronology, and geodynamic evolution: *Precambrian Research*, v. 141, p. 83–105.
- Klein, E.L., Moura, C.A.V., and Pinheiro, B.L.S., 2005c, Paleoproterozoic crustal evolution of the São Luís craton, Brazil: Evidence from zircon geochronology and Sm-Nd isotopes: *Gondwana Research*, v. 8, p. 177–186.
- Klein, E.L., Harris, C., Renac, C., Giret, A., Moura, C.A.V., and Fuzikawa, K., 2006a, Fluid inclusion and stable isotope (O, H, C, and S) constraints on the genesis of the Serrinha gold deposit, Gurupi belt, Northern Brazil: *Mineralium Deposita*, v. 41, p. 160–178.
- Klein, E.L., Moura, C.A.V., and Harris, C., 2006b, Stable (O, H, C, S) and radiogenic (Pb) isotopes evidence for the genesis of orogenic gold deposits of the Gurupi belt, Brazil: Facultad de Agronomía y Facultad de Ciencias, Universidad de la Republica, South American Symposium on Isotope Geology, 5th, Punta del Este, Uruguay, Short Papers, p. 500–503.
- Klein, E.L., Harris, C., Giret, A., and Moura, C.A.V., 2007, The Cipoeiro gold deposit, Gurupi belt, Brazil: Chlorite geochemistry, and stable isotope study: *Journal of South American Earth Sciences: Journal of South American Earth Sciences*, v. 23, p. 242–255.
- Kranidiotis, P., and MacLean, W.H., 1987, Systematics of chlorite alteration at the Phelps Dodge massive sulfide deposit, Matagami, Quebec: *ECONOMIC GEOLOGY*, v. 82, p. 1898–1911.
- Lambert, I.B., Phillips, G.N., and Groves, D.I., 1984, Sulfur isotope compositions and genesis of Archaean gold mineralization, Australia and Zimbabwe, in Foster, R.P., ed., *Gold'82: The geology, geochemistry and genesis of gold deposits*: Geological Society of Zimbabwe Special Publication, v. 1, p. 373–387.
- Marcoux, E., and Milési, J.P., 1993, Lead isotope signature of Early Proterozoic ore deposits in Western Africa: Comparison with gold deposits in French Guiana: *ECONOMIC GEOLOGY*, v. 88, p. 1862–1879.
- Matsuhisa, Y., Goldschmit, J.R., and Clayton, R.N., 1979, Oxygen isotope fractionation in the system quartz-albite-anorthite-water: *Geochimica et Cosmochimica Acta*, v. 43, p. 1131–1140.
- McCuaig, T.C., and Kerrich, R., 1998, P-T-t-deformation-fluid characteristics of lode gold deposits: Evidence from alteration systematics: *Ore Geology Reviews*, v. 12, p. 381–453.
- McRae, M., 1950, The isotopic chemistry of carbonates and a paleotemperature scale: *Journal of Chemical Physics*, v. 18, p. 849–857.
- Mikucki, E.J., and Ridley, J.R., 1993, The hydrothermal fluid of Archaean lode-gold deposits at different metamorphic grades: Compositional constraints from ore and wallrock alteration assemblages: *Mineralium Deposita*, v. 28, p. 469–481.
- Oberthür, T., Vetter, U., Davis, D.W., and Amanor, J. 1998, Age constraints on gold mineralization and Paleoproterozoic crustal evolution in the Ashanti belt of southern Ghana: *Precambrian Research*, v. 89, p. 129–143.
- Ohmoto, H., 1986, Stable isotope geochemistry of ore deposits, in Valley, J.W., Taylor Jr, H.P., and O'Neil, J.R., eds., *Stable isotopes in high temperature geological processes*: Mineralogical Society of America, *Reviews in Mineralogy*, v. 16, p. 491–559.

- Ohmoto, H., and Goldhaber, M.B., 1997, Sulfur and carbon isotopes, *in* Barnes H.L., ed., *Geochemistry of hydrothermal ore deposits*: John Wiley, p. 517–611.
- Ohmoto, H., and Rye, R.O., 1979, Isotopes of sulfur and carbon, *in* Barnes H.L., ed., *Geochemistry of hydrothermal ore deposits*: John Wiley, p. 509–567.
- O'Neil, J.R., and Taylor, H.P. 1969, Oxygen isotope equilibrium between muscovite and water: *Journal of Geophysical Research*, v. 74, p. 6012–6022.
- Palheta, E.S.M., 2001, *Evolução geológica da região nordeste do Estado do Pará com base em estudos estruturais e isotópicos de granitóides*: Unpublished MSc thesis, Belém, Brazil, Universidade Federal do Pará, 144 p. (in Portuguese).
- Passchier, C.W. and Trow, R.A.J., 1996. *Microtectonics*: Springer, 289 p.
- Pastana, J.M.N., 1995, Programa Levantamentos Geológicos Básicos do Brasil. Programa Grande Carajás. Turiagu/Pinheiro, folhas SA.23-V-D/SA.23-Y-B. Estados do Pará e Maranhão: Companhia de Pesquisas de Recursos Minerais (CPRM), 205 p.
- Phillips, G.N., and Powell, R., 1993, Link between gold provinces: *ECONOMIC GEOLOGY*, v. 88, p. 1084–1098.
- Ramboz, C., Pichavant, M., and Weisbrod, A., 1982, Fluid immiscibility in natural processes: Use and misuse of fluid inclusion data. II. Interpretation of fluid inclusion data in terms of immiscibility: *Chemical Geology*, v. 37, p. 29–48.
- Ribeiro, J.W.A., 2002, *O arcabouço estrutural da região de Chega Tudo e Cedral, NW do Maranhão, com base em sensores geofísicos*: Unpublished MSc thesis, Belém, Brazil, Universidade Federal do Pará, 155 p. (in Portuguese).
- Robert, F., and Poulsen, K.H., 2001, Vein formation and deformation in greenstone gold deposits: *Reviews in Economic Geology*, v. 14, p. 111–155.
- Roedder, E., 1984, Fluid inclusions: *Reviews in Mineralogy*, v. 12, 644 p.
- Romberger, S.B., 1990, Transport and deposition of gold in hydrothermal systems, *in* Robert, F., Sheahan, P.A., and Green, S.B., eds. *Greenstone gold and crustal evolution*: NUNA Conference Volume, Geological Association of Canada, p. 61–66.
- Sharp, Z.D., and Kirchner, D.L., 1994, Quartz-calcite oxygen isotope thermometry: A calibration based on natural isotopic variations: *Geochimica et Cosmochimica Acta*, v. 58, p. 4491–4501.
- Shepherd, T.J., Rankin, A.H., and Alderton, D.H., 1985, *A practical guide for fluid inclusion studies*: Glasgow, Blackie, 239 p.
- Sheppard, S.M.F., 1986, Characterization and isotopic variations in natural waters, *in* Valley, J.W., Taylor, H.P., and O'Neil, J.R., eds., *Stable isotopes in high temperature geological processes*: Mineralogical Society of America, *Reviews in Mineralogy*, v. 16, p. 165–183.
- Sibson, R.H., 2001, Seismogenic framework for hydrothermal transport and ore deposition: *Reviews in Economic Geology*, v. 14, p. 25–50.
- Span, R., and Wagner, W., 1996, A new equation of state for carbon dioxide covering the fluid region from the triple-point temperature to 1100 K at pressures up to 800 MPa: *Journal of Physics and Chemical Reference Data*, v. 25, p. 1509–1596.
- Spicuzza, M.J., Valley, J.W., Kohn, M.J., Girard, J.P., and Fouillac, A.M., 1998, The rapid heating, defocused beam technique: A CO₂-laser-based method for highly precise and accurate determination of $\delta^{18}\text{O}$ values of quartz: *Chemical Geology*, v. 144, p. 195–203.
- Torquato, J.R., and Cordani, U.G., 1981, Brazil-Africa geological links: *Earth-Science Reviews*, v. 17, p. 155–176.
- Torresini, C., 2000, *The Gurupi gold deposits (Cipoeiro and Chega Tudo), Gurupi belt, Pará, Brazil; geology and mineralization*: Sociedade Peruana de Geologia International Gold Symposium, 4th, Lima, Peru, *Anal. (on CD-ROM)*.
- Vennemann, T.W., and O'Neil, J.R., 1993, A simple and inexpensive method for hydrogen isotope and water analyses of minerals and rocks based on zinc reagent: *Chemical Geology, Isotope Geoscience Section*, v. 103, p. 227–234.
- Villas, R.N.N., 1982, *Geocronologia das intrusões ígneas na bacia do rio Guamá, nordeste do Estado do Pará*: Sociedade Brasileira de Geologia-Núcleo Norte, Simpósio de Geologia da Amazônia, 2nd, Belém, Brazil, v. 1, p. 233–247.
- Witt, W.K., 1993, Lithological and structural controls on gold mineralization in the Archaean Menzies-Kambalda area, Western Australia: *Australian Journal of Earth Sciences*, v. 40, p. 65–86.
- Wood, S.A., 1998, Calculation of activity-activity and log f_{O_2} -pH diagrams: *Reviews in Economic Geology*, v. 10, p. 81–96.
- Yamaguti, H.S., and Villas, R.N.N., 2003, Estudo microtermométrico dos fluidos hidrotermais relacionados com a mineralização aurífera de Montes Áureos, NW do Maranhão: *Revista Brasileira de Geociências*, v. 33, p. 21–32.
- Yardley, B.W.D., and Graham, J.T., 2002, The origins of salinity in metamorphic fluids: *Geofluids*, v. 2, p. 249–256.
- Zhang, Y.G., and Frantz, J.D., 1987, Determination of the homogenization temperatures and densities of supercritical fluids in the system NaCl-KCl-CaCl₂-H₂O using synthetic fluid inclusions: *Chemical Geology*, v. 64, p. 335–350.
- Zheng, Y.F., 1993, Calculation of oxygen isotope fractionation in hydroxyl-bearing silicates: *Earth and Planetary Science Letters*, v. 120, p. 247–263.